Sustainable Energy & Fuels

ROYAL SOCIETY OF CHEMISTRY

PERSPECTIVE

View Article Online
View Journal | View Issue

Cite this: *Sustainable Energy Fuels*, 2025, **9**, 5811

Progress and perspectives on gas diffusion layers for proton exchange membrane fuel cells with high power density: from structural engineering to component integration

Qinglin Wen[a] and Xiaochun Zhou *[ab]

Received 19th April 2025
Accepted 4th September 2025

DOI: 10.1039/d5se00552c

rsc.li/sustainable-energy

Proton exchange membrane fuel cells (PEMFCs) are at the forefront of sustainable energy technologies, offering clean and efficient energy conversion powered by renewable sources. The gas diffusion layer (GDL), an important component of PEMFCs, plays a pivotal role in facilitating gas and water transport, electron conduction, and thermal management between the catalyst layer (CL) and the bipolar plate. The discharge performance and power density of PEMFCs are significantly affected by the properties of the GDL. In this perspective, we focus on strategies for optimizing the bulk structure of the GDL, specifically engineering pore architecture and wettability. Meanwhile, from the aspect of relationships between the GDL and other components, we highlight the influence of the GDL surface structure on the CL|GDL interface and summarize the progress in integrated GDL and flow field (integrated GDL|FF) designs. These advancements promote efficient mass transport and enhance the overall performance of PEMFCs. Moving forward, we anticipate that GDL advancements will evolve synergistically with next-generation membrane electrode assemblies, ultimately enabling a new class of highly integrated PEMFC stacks.

1. Introduction

Proton exchange membrane fuel cells (PEMFCs) are emerging as one of the most promising energy conversion technologies, offering high efficiency, short fueling times, and low carbon emissions while powering electrical devices and transportation without pollution.[1,2] Currently, several vehicles use hydrogen PEMFCs as the power sources.[3] Among them, the second-generation Toyota Mirai with 5.4 kW L^{-1} volumetric power density and an operating current density above 2 A cm^{-2} stands as the most representative example.[4,5] Despite this, the operating current density and power density must be further improved to accelerate the commercialization of PEMFCs. According to the fuel cell stack performance roadmap by Japan's New Energy and Industrial Technology Development Organization (NEDO), the current density and volumetric power density targets are set to reach 3.8 A cm^{-2} and 6.0 kW L^{-1} by 2030, with further improvements to 4.0 A cm^{-2} and 9.0 kW L^{-1} by 2040.[6,7] The increase in current density and power density will introduce significant challenges to the structural designs of the components in PEMFCs.

Typically, a PEMFC consists of four main components, including a proton exchange membrane (PEM), catalyst layer (CL), gas diffusion layer (GDL) and bipolar plate with flow field (FF), as shown in Fig. 1a. The hydrogen oxidation reaction occurs in the anode CL and the oxygen reduction reaction occurs in the cathode CL. The PEM conducts protons from the anode to the cathode and isolates hydrogen and oxygen. The GDL, composed of a gas diffusion backing (GDB) and a microporous layer (MPL), and the bipolar plate provide functions of electron conduction, gas transfer, water transport, heat release, *etc.* These components are both made into thin and planar structures that maximize the surface-to-volume ratio to provide large reaction surfaces and short transport pathways.[8] In practical applications, multiple single PEMFC units are assembled into a stack to achieve the desired voltage and output power as Fig. 1b shows. Therefore, there are two ways to increase the volumetric power density of PEMFC stacks to meet commercial requirements, including improving the power density and reducing the volume.

Optimizing the structure and properties of the GDL is crucial for enhancing the performance of PEMFCs. The increase in power density of PEMFCs is limited by activation polarization, ohmic polarization and concentration polarization as illustrated by the typical polarization curve shown in Fig. 1c.[9] The GDL, which connects the CL to the bipolar plate and plays an important role in transporting gas, water, electrons and heat, as shown in Fig. 1d, has a significant impact on the ohmic

---

[a] *Division of Advanced Nanomaterials, Suzhou Institute of Nano-tech and Nano-bionics, Chinese Academy of Sciences (CAS), Suzhou, 215123, China. E-mail: xczhou2013@sinano.ac.cn*

[b] *Nano Science and Technology Institute, University of Science and Technology of China, Suzhou, 215123, China*

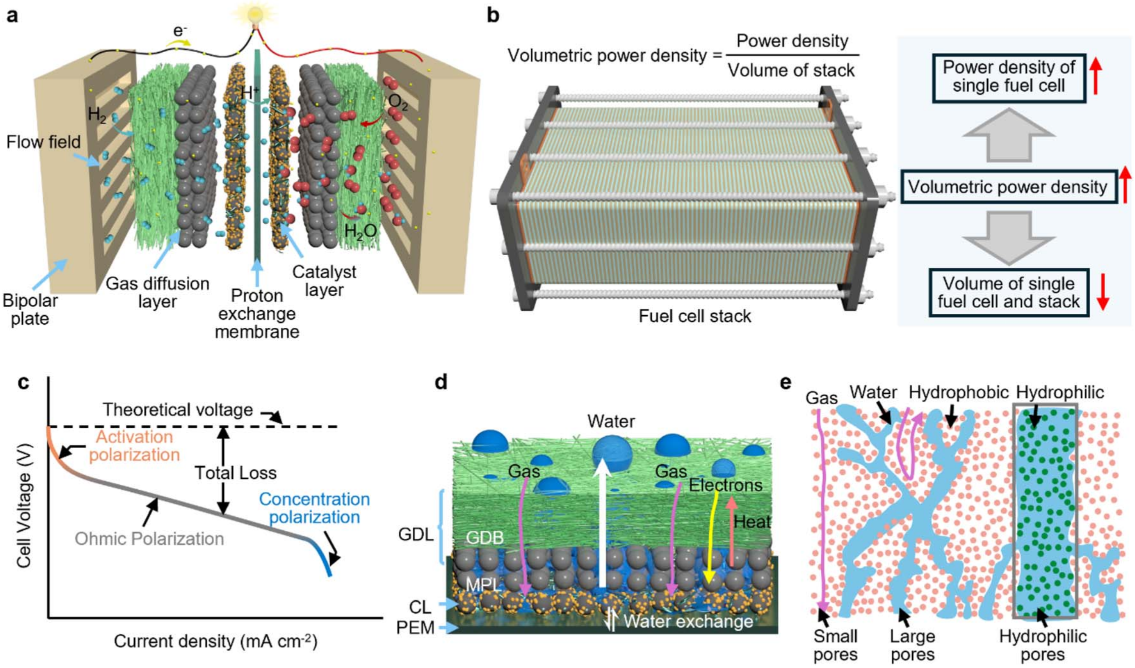

Fig. 1 Fundamentals of a PEMFC and GDL. (a) The structure of a PEMFC. (b) The volumetric power density of the PEMFC stack. (c) The typical polarization curve of a PEMFC. (d) Functions of a GDL. (e) Water transport in a GDL.

polarization and concentration polarization of PEMFCs.[10] The resistances of the GDL, including its bulk resistance and contact resistance at the interface of the CL and bipolar plate, are significant contributors to ohmic resistance.[11,12] Meanwhile, the GDL is responsible for transporting gas and water between the bipolar plate and CL, which has a great impact on mass transfer resistance.[13] To achieve the above functions, highly porous materials with favourable electrical conductivity and gas permeability are chosen as the primary materials for GDLs. The porous materials used as GDBs include carbon paper, carbon cloth, carbon felt, metal foam, metal mesh, *etc.*, in which carbon paper made by paper-making methods with fantastic mechanical properties and corrosion resistance has become the most widely used material.[14] The MPL consisting of nanoporous carbon black and hydrophobic agents is directly coated on one side of the GDB by spraying, blade coating, slot die coating, screen printing, *etc.*[15] This exemplary GDL structure currently stands as the most commercially viable solution in the industry.

Nevertheless, there still remains significant potential to enhance the performance of PEMFCs by optimizing the GDL structure, which contributes to high contact resistance and mass transfer resistance, particularly at high current densities. From the perspective of the GDL itself, tortuous and highly hydrophobic pores are not conducive to water and gas transport at high current density and can easily cause severe concentration polarization.[16,17] Liquid water tends to accumulate in the electrode due to high breakthrough pressure and easily occupies larger pores with low capillary forces, causing a large number of gas transport channels to be blocked, as shown in Fig. 1e. In terms of the relationships between the GDL and other components, surface defects (such as cracks) and roughness result in poor interface contact between the GDL and CL, resulting in high contact resistance and promoting the risk of water accumulation.[18,19] To improve the power density of PEMFCs, the above issues are required to be taken seriously to minimize the resistance of the GDL on electron and mass transfer.

Reducing the volume of the PEMFC stack is another important way to increase volumetric power density. As the PEM becomes thinner, the current GDL and flow field plate account for more than 95% of the PEMFC thickness. In fact, the functions of the two overlap significantly, such as transporting gases, water, electrons, and heat. Additionally, the interface where the GDL contacts the solid ribs on the bipolar plate is a dead zone for gas flow and thus the regions beneath the ribs are also prone to liquid water accumulation, resulting in a larger mass transfer resistance.[18,20,21]

In this perspective, we summarized strategies for optimizing the pore structure and wettability to enhance gas and water transport efficiency regarding the structure of the bulk GDL. From the relationship between PEMFC components, we summarized the optimization of the CL|GDL surface structure and integration of the GDL and flow field. We also discussed the mechanisms underlying enhanced water and gas transport at high current densities in PEMFCs and the resultant improvements in peak power density. This perspective offers insights into the regulation strategies and developments of future GDLs, aiming to highlight the importance of structural optimization in GDLs.

2. Designing and engineering pore morphology in the GDL for enhanced power density

The pores of the GDL are its most critical structure, as they provide transport pathways for both gases and water. Inevitably, the efficiency of gas and water transport within the pores of the GDL, as well as the mutual interference between them, significantly impact the performance of PEMFCs. The gas transport in the GDL and the capillary force-driven water transport are highly dependent on pore size and its distribution. Therefore, rationally optimizing the pore structure of the GDL plays a positive role in improving the performance of PEMFCs.

2.1. GDL with an ordered pore structure

The GDL must be a highly porous material with favorable electrical conductivity, of which carbon fiber paper is widely used as a raw material due to its excellent mechanical properties and corrosion resistance and will remain as the primary GDB for the near future. However, the arrangement of carbon fibers is disordered in carbon fiber paper, resulting in disordered pore size and distribution.[16] In addition, in order to improve the contact between the GDL and the catalyst layer and reduce the difference in pore size between the two, a MPL consisting of carbon black and polytetrafluoroethylene (PTFE) is universally coated on one side of the carbon paper.[11,22] The pores of the MPL are formed by the piles of carbon black particles, which are also badly disorganized to provide tortuous transport paths for both reactant gas and water. In a hydrophobic GDL, liquid water is first accumulated, leading to a pressure buildup until the breakthrough pressure is reached, after which it is drained through the pores.[23] Therefore, most of the pores in the MPL and GDB are easily filled or partially blocked by liquid water, resulting in tortuous, low efficient and unstable transport of both water and reactant gas. At high current density, the pores that can serve as effective gas transport channels are greatly reduced and the CL cannot receive a sufficient gas supply to satisfy the demand for generating a higher current density.

The tortuosity of the pore structure in conventional GDLs causes tortuosity in the gas and water transport pathways. Adopting alternative GDLs with ordered pores to minimize tortuosity is expected to enhance the mass transfer in PEMFCs to a great extent.[24–26] By constructing models for carbon paper with a random pore structure, as well as cubic lattice (isotropic) and hexagonal lattice (anisotropic) GDBs with ordered pore structures, as shown in Fig. 2a, Daniel *et al.* simulated the effect of ordered pore structure design on GDB mass transfer in PEMFCs.[24] Both ordered micro-structures have higher through-plane permeability than the carbon paper GDL. Compared with the chaotic water and gas transport in conventional GDLs (Fig. 2b1), ordered pore structure design in GDBs significantly reduces the tortuosity of the transport channels (Fig. 2b2), allowing straightforward transport of oxygen and water. As a result, optimal oxygen delivery to the electrodes is achieved. In order to verify the effect of this idealized pore structure regularity of the GDB on mass transfer in PEMFCs, Daniel *et al.* further obtained a polymer framework with a regular and ordered pore structure by 3D printing resin and then obtained a carbon material GDB with a highly ordered pore structure after carbonization and hydrophobicity treatment.[25] The MEA composed of a 3D-printed GDB with highly ordered pores is shown in Fig. 2c. Although 3D-printed GDBs have lower power density and greater impedance than carbon paper because of higher hydrogen cross-permeation, based on electrochemical properties they concluded that 3D-printed GDBs exhibit lower mass transfer resistance and better water management than carbon paper. The superior mass transfer of 3D-printed GDBs with regular pore structures has also been validated in other similar electrochemical devices, such as anion exchange membrane fuel cells and water electrolyzers.[27–29]

While 3D printing technology holds significant promise for constructing carbon material structures, it still requires further advancements in large-scale and massive production.[36] In contrast, machined metal sheets and metal meshes are easy to process and have a regular pore structure as well.[37–39] Shiro *et al.* reduced the ohmic resistance and mass transfer loss of PEMFCs by replacing the carbon paper GDL with a perforated metal sheet with a MPL.[39] The limiting current density of PEMFCs has been increased from above 2.0 A cm^{-2} to above 2.5 A cm^{-2}. Although this structure has regular pores, it is generally a solid state that does not allow gas transport in the in-plane direction. Furthermore, due to the large through-pores, the MPL is easily filled into the pores.[39] Therefore, there is still a lack of a suitable preparation strategy for GDLs with ideal ordered pore structures.

2.2. GDL with a hierarchical pore structure

A GDL with an ideal regular pore structure has little application value due to the lack of a suitable preparation method and sufficient verification of its performance and stability in PEMFCs. To overcome the tortuous transport channels and the sharing of water and gas transport channels caused by the disordered pores in a conventional GDL, other feasible methods for improving the pore structure ro improve the mass transfer efficiency and reduce the influence of water on gas transfer are eagerly desired. The hierarchical pores of distinctly different sizes can effectively enhance water and gas transport in the GDL. As shown in Fig. 2d, the hierarchical pores in the GDL can be constructed either in GDB or MPL, or throughout the entire GDL. Due to the difference in capillary force, liquid water tends to be transported through large pores with low capillary force, while the reactant is transported through small pores with high capillary force that liquid water is hard to invade.[40–42]

Hierarchical pores can be introduced in GDBs by laser perforation.[31,43–45] Christoph *et al.* fabricated carbon paper with a regular slit-type pore structure using laser perforation as a GDL (uncoated MPL) and investigated the effect of perforated area on PEMFC performance.[31] Since liquid water tends to be transported through the large-sized pores, perforated structures can substantially improve water transport, which leads to an

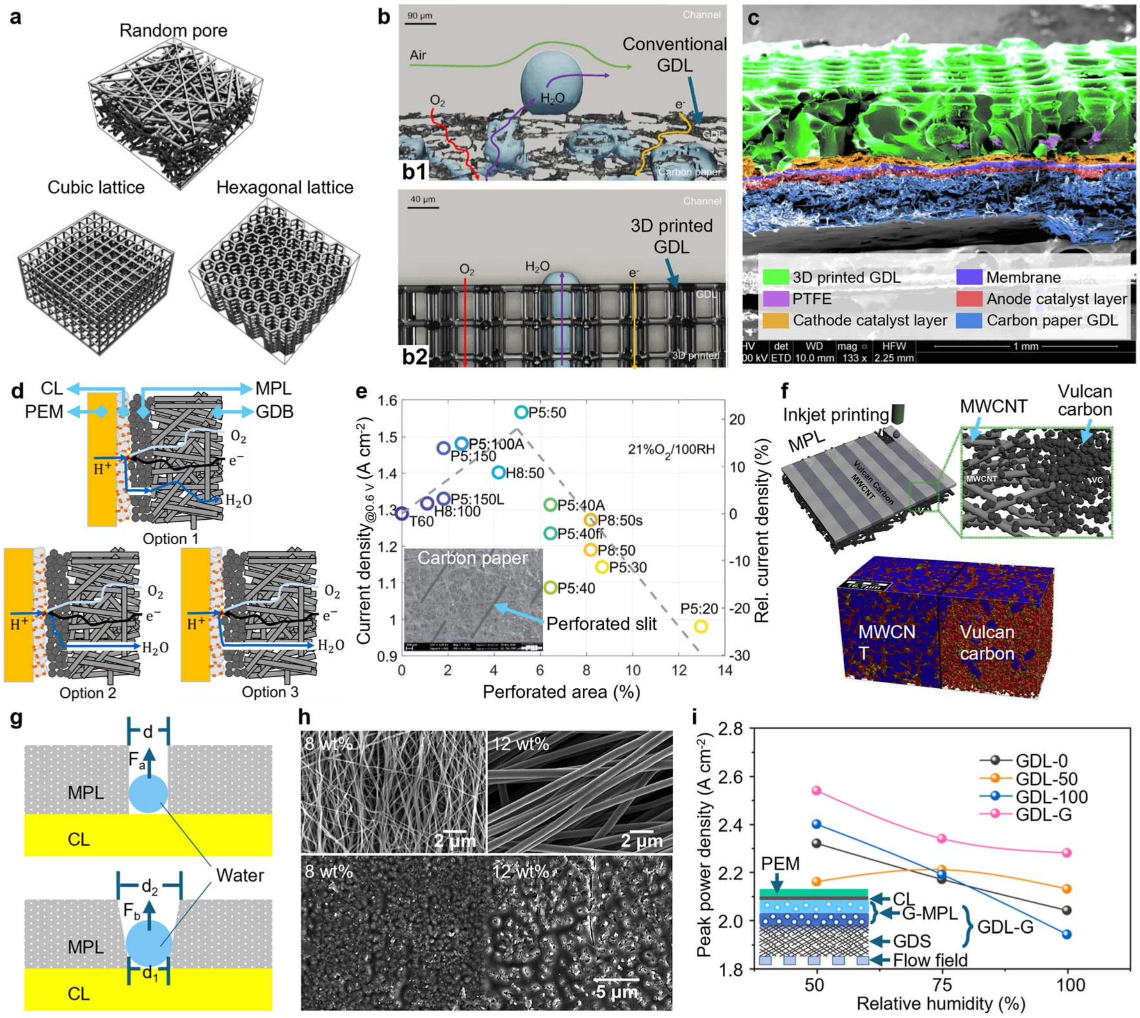

Fig. 2 The design strategies for the pore structure of GDLs. (a) Models for the GDL with ordered pores.[24] Copyright 2019 IOP Publishing. (b) Gas and water transport in (b1) a conventional GDL and (b2) a 3D-printed GDL with ordered pores.[25] Copyright 2022 Elsevier. (c) PEMFC of a 3D-printed GDL with ordered pores.[25] Copyright 2022 Elsevier. (d) Schematic images of GDLs with hierarchical pore structures in (Option 1) a perforated MPL, (Option 2) a perforated GDB, and (Option 3) a perforated MPL + GDB.[30] Copyright 2022 Elsevier. (e) PEMFC performance of GDBs with different perforated areas.[31] Copyright 2022 Royal Society of Chemistry. (f) The hierarchical pore structure in a MPL prepared by inkjet printing.[32] Copyright 2020 Elsevier. (g) Liquid water transport in a straight pore and gradient pore.[33] Copyright 2007 Elsevier. (h) SEM images of a MPL with gradient pore size prepared by electrospinning.[34] Copyright 2020 American Chemical Society. (i) The PEMFC performance of a MPL with gradient pore size prepared using pore formers.[35] Copyright 2024 American Chemical Society.

enhanced mass transfer. Furthermore, they investigated the role of slit perforation in drainage within the PEMFC using *operando* dynamic X-ray tomographic microscopy.[46] The findings indicated that the slits contributed to water collection and facilitated water redistribution in the GDL, thereby enhancing gas and water transport in the PEMFC and enabling a higher discharge current density. However, it is not true that GDLs with more and larger perforations are better for PEMFC performance. Despite the significant improvement in mass transfer, too many oversized perforated structures can lead to excessive water loss, resulting in a reduction in proton conductivity. According to their studies, 5% perforation area has the most significant increase by up to 20% in power density, as shown in Fig. 2e.[31] Lin *et al.* similarly showed that quadrilateral patterned perforations were able to increase the current density of the PEMFC by 28.6% to 5.4 A cm^{-2} with a peak power of 1.43 W cm^{-2} through enhanced water transport.[44]

Although the pores with higher capillary force in the MPL can significantly reduce the saturation of liquid water in the GDL, the MPL also faces severe obstruction of water and gas transport at high current density.[47,48] Because of the similar capillary forces, liquid water generated in the cathode CL does not merge in the MPL with only nanometer-sized pores, and there are a large number of breakthrough points at the MPL|GDB interface after liquid water penetrates the MPL.[49] Therefore, most of the pores in the MPL and GDB are filled or partially blocked by liquid water, resulting in tortuous, low efficient and unstable transport of both water and reactant gas. The introduction of larger micron-sized pores (which exhibit low capillary force) into the MPL with nanometer-sized pores (with high capillary force) enables a classification of capillary forces. This design encourages the preferential transport of liquid water through the larger pores, where the capillary forces are weaker. The larger pores in the MPL also merge the transport pathways for the substantial amounts of liquid water generated in the CL.[49] This reduces the number of breakthrough points for water entering the MPL|GDL interface and leads to the formation of stabilized water pathways that serve as primary channels for water transport within the MPL.[50,51] The liquid water saturation in the GDB also decreases due to the more stable and regular drainage of the MPL. Furthermore, the large pores in the hierarchical structure of the MPL facilitate the drying of nanosized pores, providing stable and effective transport channels for oxygen.[32,49,52]

Cracks in MPLs, inherently providing graded pore structures, are beneficial to the enhancement of mass transfer and the improvement of power density.[53–56] However, the formation of cracks is irregular, inhomogeneous and difficult to control, and more suitable graded pore structures are required to be fabricated by artificial methods.[57] The hierarchical pore structure can be constructed in MPLs using pore-making agents, such as soluble or decomposable inorganic salts, thermally decomposable polymers, *etc.*[58–62] Li *et al.* prepared MPLs with hierarchical pore channel structures by adding $CaCO_3$ to the MPL slurry and then etching it with HCl after coating.[59] Compared to a cracked MPL, the MPL with hierarchical pore sizes prepared by this method improved the concentration polarization of the PEMFC and achieved a peak power density increase from 1.15 W cm^{-2} to 1.24 W cm^{-2} owing to the enhanced mass transfer. Christopher *et al.* prepared a perforated MPL using thermally decomposable polymethyl methacrylate particles as pore formers.[61] Liquid water is allowed to transport through the large pores at very low capillary pressures, while the small pores defined by the carbon black remain water-free and act as oxygen transport channels. Finally, the perforated MPL exhibits a 45% higher current density than the commercial reference MPL due to the significantly reduced oxygen transfer resistance, and the platinum specific power density at 0.6 V is reduced by approximately 30% from $\approx 0.38\ g_{Pt}\ kW^{-1}$ to $\approx 0.26\ g_{Pt}\ kW^{-1}$. As with GDBs, the hierarchical pore structure can be constructed in MPLs by laser perforation.[63] Additionally, since MPLs are prepared by coating, the pore size distribution in different regions can be planned by selective coating. Insung *et al.* prepared a patterned MPL with graded pore sizes in the surface by printing different slurries with and without multi-walled carbon nanotubes (MWCNTs), as shown in Fig. 2f.[32] Since the MWCNTs act as spacers between the Vulcan carbon particles, the areas with the MWCNTs have larger pore sizes. These areas are more conducive to the accumulation and removal of water, ensuring better oxygen transport to the areas without MWCNTs. As a result, the current density at 0.6 V increased from 858.6 mA cm^{-2} to a maximum of 900 mA cm^{-2}.

2.3. GDL with a gradient pore structure

The capillary force driving liquid water transport in MPLs with pore gradient structures (in which porosity or pore size increases from the CL to GDB) is lower than in MPLs with straight pore structures, as shown in Fig. 2g.[33] Therefore, hydrophobic GDLs with a gradient porosity and gradient pore structure are more conducive to drainage and mass transfer enhancement in PEMFCs. In contrast, constructing a reverse gradient pore structure in the GDB or MPL may be detrimental to the drainage and mass transfer enhancement. Gradient pore structures are usually constructed in MPLs because the production of carbon paper is complicated, and the pore structure is difficult to control.

Although it is difficult to construct gradient pores when carbon paper is formed, a combination of GDBs using different pore structures can form a porosity structure gradient as previously reported.[64,65] Hiramitsu *et al.* found that when the GDB close to the CL has a larger pore structure with low capillary force, a larger water layer is formed on the surface of the CL and prevents gas diffusion.[64] Meanwhile, when the GDB close to the CL has a smaller pore structure with high capillary force, flooding on the CL surface significantly alleviates because the formation of the water layer is suppressed and the gas transfer becomes smooth. The pore gradient in GDBs can also be achieved by other preparation methods.

In addition, the electrospinning technique, which has been applied in GDL preparation in recent years, is another promising method for the construction of porosity gradient structures.[34,66–68] The regulation of pore size in GDLs can be achieved by adjusting the concentration of the electrospinning solution that can adjust the size of the fiber diameter formed by spinning. For example, Manojkumar *et al.* obtained textiles with pore size gradients prepared by electrospinning using 8% and 12% concentrations of polyacrylonitrile solutions, which were then carbonized to obtain porous carbon materials with pore size gradients, as shown in Fig. 2h.[34] The power density of the electrospinning GDB with pore size gradients reached 0.86 W cm^{-2}, better than the 0.80 W cm^{-2} of SGL 28BC. In addition, the 3D printing adopted by Huang *et al.* also demonstrated the potential application of this technology in constructing GDBs with gradient porosity structures.[28]

MPLs with a gradient pore structure are typically created by blending different materials or various contents of pore formers into the slurry and subsequently applying multiple layers of coating.[35,60,69–71] For example, Chen *et al.* constructed MPLs with a graded pore structure and MPLs with a gradient pore structure by using different contents of NH_4Cl as the pore former.[60] MPL-40 with hierarchical pores was prepared using 40% NH_4Cl and MPL-G with a gradient pore structure was prepared using 40% NH_4Cl in the inner layer (close to GDB) and 20 wt % NH_4Cl in the the outer layer. Both of them facilitated mass transfer in PEMFCs and significantly improved the performance at high current density. Among them, MPL-G with a gradient pore structure showed a greater improvement on mass transfer. The peak power of MPL-0 without the pore former only reached 0.55 W cm^{-2}, while the peak power of MPL-G with a gradient pore structure increased to 0.627 W cm^{-2}. The MEA containing MPL-G also showed the lowest mass transfer impedance of 0.1378 Ohm cm^2, lower than the 0.1636 Ohm cm^2 of MPL-0. Wang *et al.* prepared a double-layer structural MPL with an ordered gradient pore distribution by using polyethylene glycol as a pore former.[35] The gradient pore structure of the structural MPL generated a gradient capillary pressure, which provides a driving force to facilitate water discharge, resulting in an upgraded mass transfer. Consequently, a PEMFC consisting of the double-layer MPL fed with pure oxygen had the best peak power in 50–100% RH, as shown in Fig. 2i, with the highest peak power of 2.54 W cm^{-2} at 5.77 A cm^{-2} at 50% RH.

In summary, pore structure engineering is currently the most commonly used method for optimizing GDLs. By precisely controlling the pore structure, a graded capillary pressure or capillary pressure gradient can be achieved, thereby enhancing gas and water transport performance. Nevertheless, the design of pore structures requires precise control, as unsuitable pore configurations may lead to dehydration of the ionomer, resulting in reduced discharge performance and durability. Additionally, the precision of large-scale manufacturing must be carefully managed to ensure consistency in the micro/nanoscale pore structures during mass production of GDLs. Finally, pore structure engineering must also consider the mechanical properties of GDLs to maintain structural stability under compression. Therefore, future optimization of GDL pore structures should combine multiscale simulations, advanced characterization techniques, and precise fabrication processes to achieve an accurate match between pore structure parameters and PEMFC operating conditions.

3. Engineering wettability for superior power density enhancement

The transport paths of liquid water are determined by the regions with the lowest capillary force in porous GDLs. However, current commercial GDLs are usually treated with a hydrophobic agent and exhibit strong hydrophobicity overall. In such a GDL, liquid water has tortuous paths due to the inhomogeneity of the pore geometry, and there exist some dead zones that are unable to transport either reactant gas or liquid water, as shown in Fig. 3a1.[72] Therefore, the effective pores acting as gas and water transport channels are much fewer than the actual pores of the bulk GDL. Moreover, the high capillary force in the pores of the overall hydrophobic GDL leads to a high liquid water breakthrough pressure, which means that liquid water accumulates to acquire a sufficient pressure in the electrode before it can be discharged.[23,73,74] Another frequently overlooked factor that limits concentration polarization is that the CL, primarily composed of carbon-supported Pt and perfluorosulfonic acid, is actually less hydrophobic than the GDL due to the presence of hydrophilic groups in perfluorosulfonic acid. At high current densities when water is generated fast, liquid water may preferentially accumulate in the CL causing electrode flooding and requiring specific barriers to penetrate the GDL.[75–77] Therefore, the design of the GDL should consider not only the transport of liquid water within the bulk GDL but also the effective removal of excessive water from the CL.

3.1. GDL with patterned wettability

To design the GDL effectively, it is crucial to not only consider the influence of capillary forces on water content but also control water distribution in the porous structure. By creating wettability patterns in GDLs, liquid water is preferentially transported through the hydrophilic regions, while the hydrophobic regions resist wetting, effectively functioning as efficient gas transport channels, as shown in Fig. 3a2.[72] Simultaneously, the hydrophilic capillary forces provide the driving forces that direct liquid water discharge through pores, which can significantly diminish the water breakthrough in those pores. Thus, patterned wettability in GDLs not only enhances the transport efficiency of liquid water but also minimizes its impact on gas transfer. This ultimately reduces the mass transfer resistance in PEMFCs, leading to a significant increase in peak power.

Selective hydrophilic treatments such as selective graft polymerization, selective spraying, and selective plasma treatment can build patterned wettable pores and separate water and gas transport channels in GDBs.[72,78,83–90] Antoni *et al.* partially exposed commercial carbon paper coated with hydrophobic fluorinated ethylene propylene to radiation using a mask to locally generate free radicals and then immersed it in a solution of grafted hydrophilic *N*-vinylformamide monomers.[72] Because the graft copolymerization occurred only in the areas previously exposed to the electron beam, carbon paper with patterned wettability was easily prepared by this method as illustrated by the element distribution and the state of water on the carbon paper shown in the inset images of Fig. 3b. Compared to hydrophobically treated commercial carbon paper, the carbon paper with patterned wettability exhibited lower concentration polarization at high current densities in PEMFCs, as shown in the polarization curve (Fig. 3b). Zhang *et al.* prepared carbon paper with patterned wettability pores by selectively spraying a hydrophilic reagent on hydrophobic carbon paper using a mask.[78] The capillary force in the pores of the hydrophobic area of the carbon paper was as high as 2 kPa, whereas it was only 0.3 kPa in the hydrophilic area. Due to the difference in capillary forces, the hydrophilic pores acted as water highways, which greatly improved the drainage efficiency of the MEA and the breakthrough pressure of the GDL was reduced from 13.61 to 2.96 kPa, as shown in Fig. 3c. The patterned pore structure of hydrophilic and hydrophobic synergistically reduced the transport resistance of oxygen and liquid water for more efficient mass transfer, and the power density of the PEMFC increased by 30% from 520 mW cm^{-2} to 678 mW cm^{-2}.

Patterned wettability pores can also be constructed in MPLs by introducing hydrophilic materials and selective hydrophilic treatment, mainly including scraping, spraying and plasma treatment.[91–96] Wang *et al.* prepared a patterned MPL featuring both hydrophilic and hydrophobic regions by selectively spraying a slurry with hydrophobic PTFE onto part regions of the carbon paper, followed by scraping a slurry with hydrophilic polyamide resin onto the remaining regions.[91] The hydrophilic region of the MPL could be wetted by water, while the hydrophobic region could not be wetted by water. This type of MPL

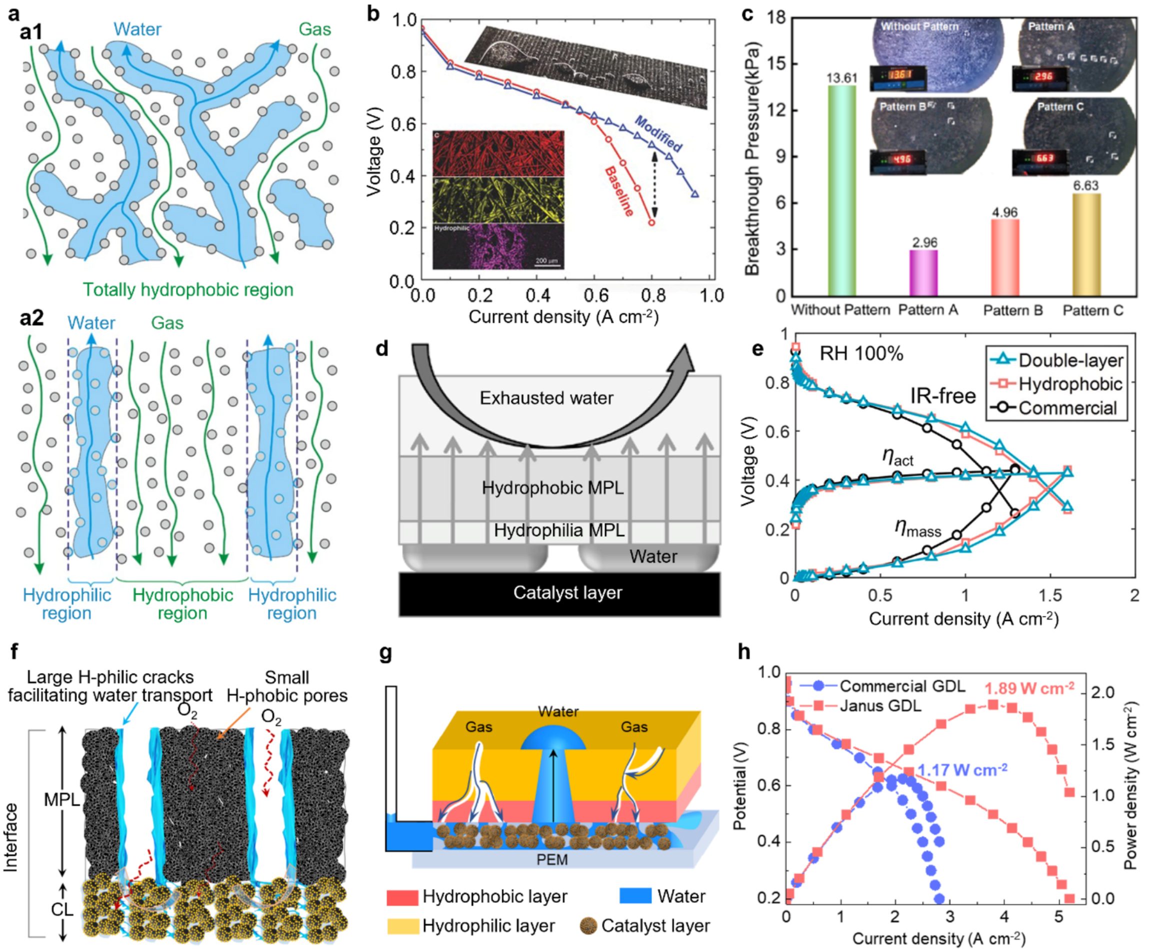

Fig. 3 Strategies for engineering wettability of GDLs. (a) Schematic diagrams of gas and liquid water transport in (a1) a hydrophobic GDL and a GDL with (a2) hydrophilic pattens.[72] Copyright 2015 John Wiley and Sons. (b) PEMFC performance of a GDL with hydrophilic pattens.[72] Copyright 2015 John Wiley and Sons. (c) The breakthrough pressure of GDLs with hydrophilic patterns.[78] Copyright 2022 American Chemical Society. (d) Schematic diagram of liquid water transport enhanced by a multi-layered GDL with different wettability.[79] Copyright 2014 Elsevier. (e) PEMFC performance of a GDL containing multiple layers prepared by electrospinning.[80] Copyright 2022 Elsevier. (f) Schematic diagram of gas and water transport within a GDL containing some large hydrophilic pores (combining engineering of the pore structure and wettability).[81] Copyright 2020 American Chemical Society. (g) Schematic diagram of gas and water transport in a Janus GDL with a wettability gradient and large perforations.[82] Copyright 2022 American Chemical Society. (h) PEMFC performance of the Janus GDL.[82] Copyright 2022 American Chemical Society.

absorbed the excessive water generated in the CL into the hydrophilic pores and transported it to the GDB, while the other hydrophobic pores were hardly wet and provided efficient transport channels for the reacting gases. Guo *et al.* prepared MPLs with patterned wettability by selectively spraying hydrophilic reagent onto some regions of hydrophobic MPLs.[92] Enhanced water management achieved by the synergistic hydrophobic and hydrophilic patterns improved mass transfer at high current density, leading to reduced concentration polarization. Therefore, the peak power of the PEMFC with the patterned MPL increases by 20% from 494.24 mW cm^{-2} to 591.36 mW cm^{-2} compared to the hydrophobic MPL.

3.2. Multi-layered GDL with different wettability

The drainage efficiency and the mass transfer of PEMFCs can also be enhanced using multi-layered GDLs with different wettability. On the one hand, the wettability gradient created by multi-layered wettability can drive the removal of liquid water. On the other hand, the absorption efficiency of GDLs for excessive water in CLs can be improved through multi-layered wettability design. The design of multi-layered wettability is focused on MPLs because they are easy to prepare and close to CLs. It is also relatively difficult to create multi-layered wettability directly on most commonly used carbon paper due to its complex preparation and large pore size.

GDBs with multi-layered wettability orifices are usually constructed by using a combination of carbon paper with different PTFE treatments.[97,98] Wang *et al.* prepared bilayer carbon paper with PTFE gradients by applying different hydrophobic treatments to TGP-H-030.[97] The results showed that the bilayer GDBs with higher inner PTFE loading reduced the saturation level of liquid water, which resulted in a higher limiting current density, smaller voltage fluctuations and more stable performance.

MPLs with multi-layered wettability pores can be prepared by coating multiple layers of carbon materials with different hydrophobicity and hydrophilicity on GDBs.[79,99,100] The multi-layered wettability includes the combinations of several layers containing different contents of hydrophobic agents or the combinations of hydrophobic and hydrophilic layers. Multi-layered MPLs with different contents of hydrophobic agents enhance water transport efficiency by constructing a hydrophobic gradient.[101–105] Pranay *et al.* coated a GDB with slurries containing 10% and 20% PTFE in sequence to obtain a double-layer MPL with a hydrophobicity gradient.[103] The MPL featuring a hydrophobicity gradient improves capillary-driven removal of liquid water and decreases its accumulation within the cathode GDB. Consequently, this significantly reduces oxygen mass transfer resistance and enhances PEMFC performance at high current densities ($\geq$1.0 A cm^{-2}). By adding a hydrophilic MPL on the hydrophobic MPL, the drainage efficiency from the CL to the GDL can be enhanced through hydrophilic capillary force, which is also beneficial for reducing the oxygen transfer resistance. Tatsumi *et al.* prepared a triple-layer MPL consisting of a hydrophilic layer, a 30% PTFE-treated hydrophobic layer and a 10% PTFE-treated hydrophobic layer, as shown in Fig. 3d.[79] The hydrophilic layer promoted water diffusion from the CL and reduced water accumulation and flooding in the CL layer. While most previous studies support placing the hydrophilic layer between the MPL and CL to enhance mass transfer, Chun *et al.* suggested positioning the hydrophilic layer between the GDB and the hydrophobic layer.[79,99,100,105,106] They proposed that when the hydrophilic layer was too close to the CL, it might trap liquid water, leading to electrode flooding.

In addition to solution coating, electrospinning precursor solution with different hydrophilic and hydrophobic substances is also an important method for preparing MPLs with multi-layered wettability. Li *et al.* prepared bilayer MPLs with gradient wettability pores by electrospinning polyvinylpyrrolidone solution with different types of carbon black.[80] The hydrophilic layer was placed between the hydrophobic layer and CL, and the bilayer MPL had the lowest concentration polarization voltage loss at 100 RH%, as shown in Fig. 3e. They also noted that the hydrophilic layer functions as a water reservoir, and an improper thickness could result in insufficient or excessive water content. This imbalance may explain why some studies have concluded that placing a hydrophilic layer between the CL and the hydrophobic layer can lead to reduced performance.

The engineering of wettability requires considering some issues that are more important in actual production and working conditions: firstly, how can current wettability regulation methods ensure the reproducibility of the structure design for high volume preparation? Secondly, since GDLs are constantly subjected to gas and water impacts and electrochemical degradation under operating conditions, how can the wettability structure be made resilient, so that the PEMFC performance has better stability and durability? Perhaps the use of hydrophobic and hydrophilic treatments that can be chemically cross-linked or have strong interactions can provide a solution.

It is worth noting that the combination of the pore structure and wettability of the GDL can be synergistically co-regulated to achieve better PEMFC performance and become the main direction for optimizing the bulk GDL in the future. Muhammad *et al.* proposed an MPL with a hierarchical pore structure and wettability to regulate water distribution in CL according to their study on the impact of pore size, wettability, and pore size distribution on liquid water transport in the cathode CL.[81] As shown in Fig. 3f, the small impenetrable hydrophobic pores maintain the hydration of the ionomer and allow oxygen transport at the CL|GDL interface, while the large hydrophilic pores are simultaneously used to efficiently remove excessive water and allow oxygen transport. Recently, we reported on the huge advantages of similar designs in improving PEMFC performance.[107] By engineering hydrophilic water transport channels inspired by plant roots with phenolic resin and microcrystalline cellulose, the liquid water breakthrough pressure of the MPL is significantly reduced from 20.7 kPa to 7.5 kPa and the capillary forces of pores are classified. Consequently, the limiting current density of the PEMFC is higher than 5 A cm^{-2} and the peak power density reaches 1.84 W cm^{-2}, which are approximately 1.42 times (only 3.77 A cm^{-2}) and 1.29 times (only 3.77 W cm^{-2}) that of the pristine MPL. Moreover, this biomimetic MPL can be produced on a large scale by the roll-to-roll method with performance similar to that of laboratory samples. Additionally, we have designed a Janus GDL with a wettability gradient and micron perforations to facilitate water and gas transport in the electrode, as shown in Fig. 3g.[82] The wettability gradient provides the driving force, and the perforations provide highly efficient paths of water transport with only 29 Pa breakthrough pressure. The efficient water transport results in significantly improved concentration polarization, as shown in Fig. 3h. Thus, the Janus GDL achieved a peak power density of 1.89 W cm^{-2} and exhibited excellent anti-flooding capacity in the PEMFC.

4. Surface structuring of the GDL to improve the CL|GDL interface

The interface between the GDL and CL also has an important influence on the performance of PEMFCs. Modulating and structuring the surface of the GDL to improve the interface between the CL and MPL is crucial for high-performance PEMFCs, among which the addition of the MPL is the most typical case. Fig. 4a shows the surface morphology of the commercial GDL SGL 39BC.[108] Generally, the pore size of the GDB is larger than 10^5 nm (Fig. 4a1), which is 3 orders of magnitude higher than that of the carbon support particles and pore size in the CL. Therefore, in PEMFCs that directly use a GDB as the GDL component, the contact between the CL and GDL is extremely poor, resulting in a large interface contact resistance and high ohmic polarization. Coating a MPL composed of carbon powder and PTFE on the GDB through methods such as spraying, blade coating, and screen printing

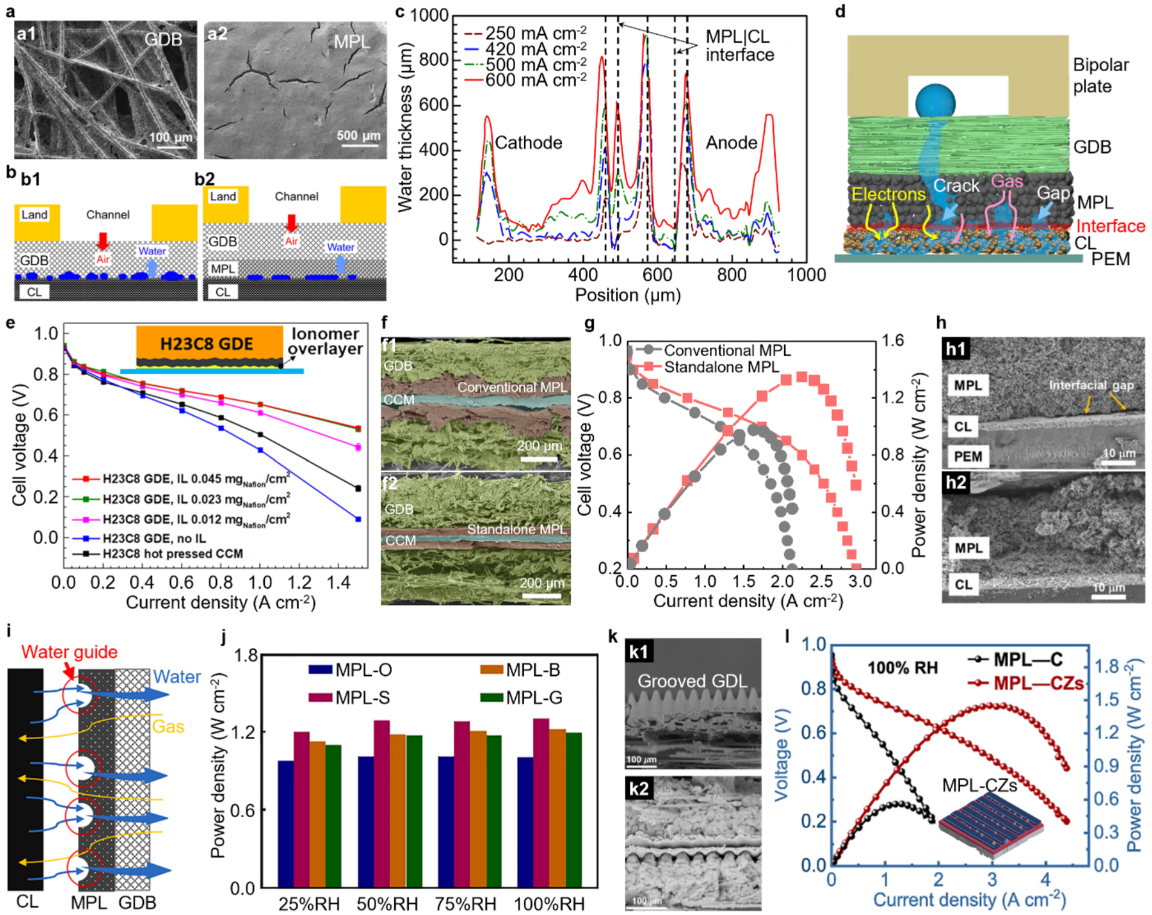

Fig. 4 Surface structure optimization of the GDL to improve the CL|GDL interface. (a) The surfaces of (a1) the GDB and (a2) the MPL of the commercial SGL 39BC.[108] Copyright 2013 IOP Publishing. (b) The water transport at the CL|GDL interface of GDLs with and without the MPL.[112] Copyright 2015 Elsevier. (c) The water distribution in PEMFCs and severe water accumulation occurring at the CL|GDL interface.[113,114] Copyright 2010 IOP Publishing, 2008 AIP Publishing. (d) The schematic diagram of the effect of the CL|GDL surface on the transport of electrons, gases, and water. (e) An ionomer overlayer to improve the surface of the CL|GDL interface.[115] Copyright 2019 American Chemical Society. (f) SEM images of PEMFCs consisting of (f1) a conventional MPL with a rough surface and (f2) a standalone MPL with a highly flat surface.[116] Copyright 2023 John Wiley and Sons. (g) The PEMFC performance of the standalone MPL.[116] Copyright 2023 John Wiley and Sons. (h) A novel CL|MPL surface *via* a MPL-attached catalyst coated membrane (CCM).[117] Copyright 2020 John Wiley and Sons. (i) Water guide at the CL|GDL interface with water guides on the MPL.[118] Copyright 2021 Elsevier. (j) The PEMFC performance of the CL|GDL interface with water guides on the MPL.[118] Copyright 2021 Elsevier. (k) SEM images of (k1) a grooved GDL with a patterned MPL and (k2) its CL|GDL interface.[119] Copyright 2019 Elsevier. (l) PEMFC performance enhanced by a grooved MPL with stripe patterns.[120] Copyright 2024 Elsevier.

can significantly reduce the pore structure on the surface of the GDL to a level comparable to that of the CL. Except for the micron cracks, there are almost entirely nanoscale pores in the MPL, which has a good match with the pore structure of the CL.[107] The addition of the MPL can significantly improve the contact between the CL and GDL, thereby reducing the interfacial contact resistance and ohmic overpotential.[109–111]

The addition of a MPL also plays an important role in improving the gas and water transport at the CL|GDL interface in PEMFCs.[121] As shown in Fig. 4b1, when a GDB is directly used as a GDL, since the capillary force in the GDB pores is significantly lower than that in the CL channels, liquid water is easily formed and accumulated on the surface of CL|GDL.[112] The interface of CL|GDL is easily covered by liquid water at high current density, and it is difficult for the reactant gas to transport through the water layer to the CL, resulting in severe concentration polarization. After the introduction of the MPL into the GDL, the difference in capillary force between the CL and MPL is small due to their similar pore sizes. Therefore, the liquid water saturation at the CL|GDL interface is reduced (Fig. 4b2), which reduces the mass transfer obstruction caused by interfacial flooding. The mitigated flooding of the CL|GDL interface by introducing a MPL has been reported in previous reports. For example, through soft X-ray radiography, Phengxay observed that the liquid water thickness at the CL|GDL interface with the SGL 24BC (with MPL) at 63 °C was 25 μm, which was much lower than the 180 μm at the SGL 24BA (without MPL) interface.[122]

The surface of a conventional MPL is not perfect although it significantly improves the contact between the CL and GDL.[123] Due to the porous structure of the GDB and the evaporation of solvent during preparation, the MPL has a large roughness and cracks are prone to appear on the surface.[57,124] Although the cracks are believed to act as liquid water transport channels, they and the rough surface of the MPL damage the interface of CL|GDL, such as by generating interfacial gaps.[96,125,126] On the one hand, liquid water easily condenses and aggregates in the gaps created by defects due to the lower capillary force (Fig. 4c).[113,114] On the other hand, these gaps lead to an imperfect contact at the interface, making the transfer channels of electrons and gases more tortuous, thereby increasing the contact resistance and mass transfer resistance at the interface (Fig. 4d).[127] In addition, it has also been investigated that the CL|GDL interfacial gap brought about by surface defects causes inhomogeneous water content distribution and stress distribution, which accelerates the aging of MEAs and deteriorates the durability of PEMFCs.[128–130]

To overcome the unfavorable effects of PEMFC performance and durability due to MPL surface defects, methods to improve the CL|GDL interface were devised. Coating a CL directly onto a GDL by the gas diiffusion electrode (GDE) method usually leads to a good CL|GDL interface. On this basis, the PEMFC with high performance can be obtained by hot pressing or applying an ionomer layer on a GDE.[112,115,131–135] Li *et al.* controlled the surface morphology of the MPL by hot pressing, which reduced the roughness of the MPL surface and improved the CL|GDL interface, enabling the GDE to achieve comparable performance to the CCM.[131] However, since the GDE usually has poor contact with the PEM, the CL|PEM interface requires to be further strengthened for better proton conduction. Wang *et al.* prepared PEMFCs with good interfaces by adding an ionomer overlayer to the GDE surface, followed by hot pressing.[115] As shown in Fig. 4e, this method drastically improves the effect of GDL surface roughness on the interface, resulting in a PEMFC performance that far exceeds that of conventional GDEs and CCMs.

The preparation of GDLs with highly flat surfaces is another important method to improve the CL|GDL interface, in which sheet MPLs are very advantageous. Sheet MPLs are usually molded directly without GDBs and are commonly prepared by compression, electrospinning, chemical vapor deposition, vacuum filtration, *etc.*[67,116,136–140] Fig. 4f shows a PEMFC assembled with standalone MPLs prepared by vacuum filtration that we previously reported.[116] Fig. 4f1 exhibits a PEMFC composed of a conventional MPL prepared by screen printing, a method capable of preparing a flat surface. There are some defects on the surface of the conventional MPL that cause some gaps at the CL|GDL interface. In contrast, the standalone MPL with a flat surface has good contact with the CL at the interface (Fig. 4f2). As a result, the PEMFC with a standalone MPL has lower internal resistance and mass transfer impedance, and the peak power increases by 38% to 1.35 W cm^{-2} (Fig. 4g). The flat surface of the sheet MPL can not only make a breakthrough in performance but is also expected to enable the MEA to have uniform stress distribution and enhance the durability of the PEMFC.[117]

Due to the more advanced CL|PEM interface, a CCM has replaced the GDE approach for large-scale industrial applications. The CL|GDL interface can also be significantly improved by a new architecture directly attaching a MPL to the CCM.[141–143] Daniel *et al.* constructed this kind of CL|GDL architecture by spraying a MPL on the cathode side of the CCM.[117] As shown in Fig. 4h1, there are inevitably some interface gaps at CL|GDL interfaces in the PEMFC prepared with conventional MPLs and CCMs. In contrast, in the novel CL|GDL architecture, there is perfect contact between the CL and MPL (Fig. 4h2). Therefore, the ohmic resistance of the PEMFC was reduced from ∼65 to ∼45 mOhm cm^2, and water flooding at the CL|MPL interface was mitigated, resulting in a significantly improved overall polarization performance. It is worth noting that there may be some concerns regarding the use of a CCM to attach the MPL. The residual surfactant in the MPL is difficult to remove and the uniform distribution of PTFE in the MPL is difficult because the CCM cannot be calcined at 350 °C, which may affect the hydrophobicity and its stability of the MPL.

While MPL surface inhomogeneities may have an impact on performance and stability, some rational structural designs have been reported to improve the performance of PEMFCs. Creating pits on MPL surface as liquid water guide can improve gas transport in PEMFCs.[118] As shown in Fig. 4i, liquid water first tends to be stored in the water guide due to lower capillary forces, avoiding occupying the gas transport pores, and then is removed more efficiently. By regulating polymethyl methacrylate, Lin *et al.* created water guides with 8 μm (MPL-S), 18 μm (MPL-B) and mixed sizes (MPL-G) on the MPL surface.[118] After the introduction of water guides, the performance of the PEMFC was improved in the range of 25–100% RH. Nevertheless, MPL-S with 8 μm water guides has the best performance (maximum 1.30 W cm^{-2} at 100% RH) in the whole humidity range due to the poorer CL|GDL interfacial contact and higher interfacial water content caused by the larger size of water guides in MPL-B and MPL-G. In addition, the authors provide durability tests to demonstrate that MPL-S has good stability while the larger water guide in MPL-B and MPL-G has a negative impact on stability. Therefore, the surface engineering of the MPL requires great attention to the precise control of size to prevent the resulting large roughness from reducing the performance and durability of PEMFCs.

In addition to introducing pits onto the MPL surface as water guides, preparing a MPL with grooves or a similar structure has also been proven to improve the performance of PEMFCs.[119,120,144–148] Jericha *et al.* created grooves on the GDL surface using a picosecond laser, as shown in Fig. 4k1.[119] These grooves significantly increase the effective surface area for Pt catalyst deposition (Fig. 4k2), which is beneficial for reducing the thickness of the CL and achieving good proton transport and good gas transport. The grooves on the GDL surface can also be expected to drive water transport. Lee *et al.* introduced ditches on the MPL surface using a nanosecond-pulse laser.[144] When the groove ditches are perpendicular to the flow channels, the performance is significantly improved due to the promotion of mass transfer under the rib area. Wang *et al.* also prepared a grooved MPL with a stripe pattern of 1 mm wide and 1 mm spacing near the catalyst layer to accumulate liquid water at the interface and then drain out smoothly over time.[120] Therefore, the peak power density of a PEMFC assembled with the grooved MPL reaches up to 1.50 W cm^{-2} at 100 RH%, as shown in Fig. 4l. It is noteworthy that the GDL with a grooved structure on the MPL surface can be easily prepared using other methods. Chen *et al.* fabricated a wavy-GDL containing wavy MPL using a wire winding bar in the MPL coating process.[145] The PEMFC with a wavy-GDL exhibits good performance in the humidity range of 20 RH% to 100% and reaches the optimum of 1.128 W cm^{-2} at 70 RH% because the wavy-GDL accelerates the exchange of reactant gases and produced water in the MEA.

Since the design of the CL|GDL interface involves both the GDL and the CL, particular attention must be paid to the properties of the CL and the correlations between the two components, especially regarding compatibility issues between hydrophilic/hydrophobic GDL designs and ionomer proton conduction. The transport process of liquid water from its generation in the CL to its expulsion through the GDL is driven by capillary forces. Rational design of the capillary force gradient can prevent excessive liquid water accumulation in the CL, thereby reducing mass transfer resistance. A typical optimization strategy for capillary forces involves inserting a hydrophilic layer between the CL and the hydrophobic GDL to effectively facilitate water transport in the CL.[149,150] However, it should be noted that proton conduction through the ionomer in the CL relies on water hydration.[151] Therefore, when designing the GDL, the conductivity of the ionomer must also be considered. Excessively reducing the water content in the CL will lead to insufficient hydration of the ionomer, hindering proton transport and consequently compromising the stability and durability of the PEMFC.[152]

Future developments in CL catalysts will focus on two key directions: ultra-low-loading Pt-based catalysts and non-precious metal CLs.[153] Ultra-low Pt-loading CLs are extremely thin, placing higher demands on the CL|GDL interface to achieve low interfacial resistance and mass transfer resistance. Additionally, the thin CL can hold significantly less water, necessitating more efficient water removal to sustain high current densities. Non-precious metal CLs typically have higher loadings and greater thickness, making effective gas transport and water drainage critical for PEMFC performance.[154] However, there is currently almost no research on GDLs tailored for ultra-low Pt-loading or non-precious metals, which warrants greater attention from the research community.

In recent years, the structures of CLs and MEAs have been optimized to enhance performance, with ordered MEAs emerging as a promising next-generation PEMFC technology.[155,156] Ordered MEAs are fabricated by constructing ordered structures on the PEM or CL. Ideally, ordered MEAs can improve catalyst utilization, expand the triple-phase reaction interface, and enhance proton, electron, gas, and water transport. However, in practice, ordered MEAs often underperform in mass transfer and are prone to flooding. The primary reason for this may be that these ordered MEAs overlook the influence of the CL|GDL interface, such as gaps and wettability mismatches. This observation appears to be validated by our recent study on an occlusal ordered MEA composed of an arrayed PEM and perforated titanium felt, which eliminates CL|GDL interface mismatches.[157] Therefore, future optimization of the CL|GDL interface should focus more on the interaction between the two components rather than optimizing either one in isolation.

5. Integrated GDL|FF for high specific power

In the current PEMFC stacks, the flow field is machined onto graphite or metal sheets to prepare the bipolar plate (Fig. 5a1).[158] Typically, the bipolar plates are made of solid materials that are impermeable to gases to prevent the penetration of hydrogen and oxygen between adjacent MEAs. In this conventional structure, the solid ribs of the bipolar plate are too dense to permit gas permeation and the GDL under the ribs is compressed more than the flow field portion. Therefore, the transport of reactant gases under the rib is difficult and highly susceptible to liquid water accumulation, a phenomenon that has been demonstrated in neutron imaging and synchrotron X-ray tomography visualization studies.[159–161]

In order to overcome the effect of poor mass transfer on PEMFC performance under the conventional configuration rib, some researchers have shifted the flow field from the bipolar plate to the GDL. Due to the abundant porosity of the GDL, the gas in the flow channel can easily enter the porous ribs, significantly enhancing the gas transport and water transport in the PEMFC. Therefore, this novel integrated GDL|FF configuration significantly contributes to the improvement of PEMFC current density and power density. The integrated GDL|FF design may become an important component of future PEMFCs because of the great advantage in increasing the volumetric power density. Currently, integrated GDL|FF consists of two main types: a GDL with a flow field and porous carbon/metal foam, as shown in Fig. 5a.

5.1. GDL with a flow field as integrated GDL|FF

Masahiro *et al.* reported such a GDL with a flow field pattern (Fig. 5b) and developed a corresponding flat-metal separator to replace conventional bipolar plates for the first time.[162,169] The GDL with a flow field pattern achieves a current density higher than 3 A cm^{-2} and a peak power density of 1.18 W cm^{-2} as Fig. 5c shows.[163] According to their study, the rib space in the porous GDL acts as a reservoir for excess water to ensure an effective oxygen supply for the CL.[170]

The structure of the flow field in the GDL can be designed to further improve water and gas transport and enhance the performance of PEMFCs. He *et al.* engraved flow field patterns on commercial carbon paper by laser engraving methods.[164] This GDL has wavy channels and micro-tunneled ribs, as shown in Fig. 5d, that can strongly and positively affect mass transfer from two aspects. On the one hand, the flowing gas can enter the tunneled porous rib to carry away the excess condensed liquid water. On the other hand, the flow channel has a wider and more efficient oxygen convection due to the turbulence caused by the undulating surface of the waves, as shown in Fig. 5e. Thus, the peak power density reaches 1.41 W cm^{-2} under 50 kPa back pressure, as shown in Fig. 5f, and the

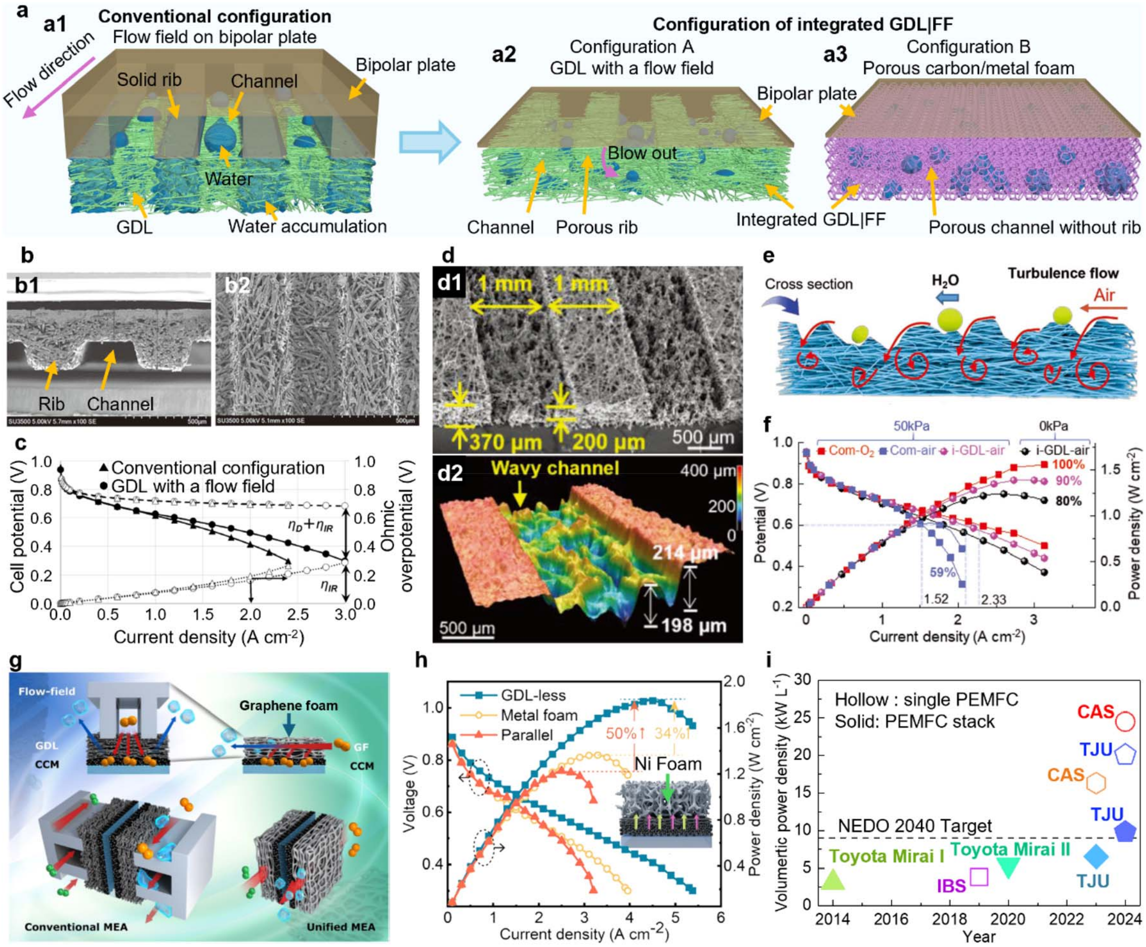

Fig. 5 The designs of integrated GDL|FFs. (a) Conventional configuration of a flow field on a bipolar plate and configurations of integrated GDL|FF including a GDL with a flow field and porous carbon/metal foam. (b) SEM images of the GDL with a flow field: (b1) cross view and (b2) front view.[162] Copyright 2022 IOP Publishing. (c) The PEMFC performance of the GDL with a flow field.[163] Copyright 2022 Elsevier. (d) Integrated GDL with wavy channels and tunnelled ribs.[164] Copyright 2023 John Wiley and Sons. (e) The schematic diagram of enhanced mass transfer achieved by integrated GDL|FF with wavy channels and tunnelled ribs.[164] Copyright 2023 John Wiley and Sons. (f) The PEMFC performance of integrated GDL|FF with wavy channels and tunnelled ribs.[164] Copyright 2023 John Wiley and Sons. (g) Graphene foam as integrated GDL|FF.[165] Copyright 2019 Elsevier. (h) Ni foam as integrated GDL|FF and its PEMFC performance.[166] Copyright 2024 Elsevier. (i) Statistical summary of volumetric power density enhanced by an integrated GDL.[164–168]

corresponding volumetric power density is as high as 16 300 W L^{-1}. In addition to the above methods, some advanced machining processes such as wire electro-discharge machining and 3D printing can also be applied to prepare the integrated GDL|FF.[171]

Although conventional MPL coating methods can be applied to integrated GDL|FF, due to structural differences in the flow field and porous ribs, the MPL may have poor uniformity and tend to penetrate the flow field. The above problems can be solved by preparing MPLs in sheet form or by directly preparing MPLs and flow field structures during the process when GDLs are molded. Sheet GDLs can be prepared directly by pressing carbon powder into sheets, chemical vapor deposition to prepare carbon nanotube sheets, electrospinning, and vacuum filtration to form conductive sheets.[67,116,136–140] Some of these methods have been realized for massive coil preparation.[107] Methods of preparing MPL and flow field patterns simultaneously have also been reported recently. By using the filter molding method, He *et al.* prepared an integrated GDL|FF consisting of a flow field, GDB and MPL.[167] The introduction of a MPL plays an important role in performance enhancement. The integrated GDL|FF with a waveform flow field achieves a power density of up to 1.63 W cm^{-2}, a 50% improvement over commercial GDLs and conventional bipolar plates, and a 146% increase in volumetric power density to 24.5 kW L^{-1}.

Although the GDL with a flow field can greatly improve the peak power of PEMFCs, there are some issues that are required to be addressed. Due to the high porosity of the GDL, the traditional flow field pattern processing method on bipolar plates cannot be directly applied to the processing of this type of flow field. Therefore, methods for massive preparation of such an integrated GDL of stack size need to be developed. Secondly, the cost of integrated GDLs needs to be reduced to an appropriate level to meet the reduction in PEMFC stack costs. In addition, during PEMFC operation, the flow channels and porous ribs are subjected to strong gas and water impacts, and whether the integrated GDL|FF can maintain long-term structural stability needs to be confirmed.

5.2. Porous carbon/metal foam as integrated GDL|FF

Since the ribs of the conventional flow field on a bipolar plate are not air-permeable, porous foam materials with interconnected pores and ultra-high porosity have been reported to replace the conventional flow field to reduce the difficulty of gas transfer and solve the problem of water accumulation under the solid ribs.[172–174] In addition, some reports have explored the use of foam materials instead of carbon paper as a GDL.[175–177] In fact, there is a great overlap between the functions of the GDL and flow field. On this basis, some researchers proposed to directly replace the existing flow field and GDL with foam materials, that is, to directly use the foam materials as integrated GDL|FF. Some simulations have demonstrated that foam materials can be used as an integrated GDL|FF in previous reports.[178,179] Due to the higher porosity, the foam used as an integrated GDL|FF has a lower pressure drop and is more conducive to the distribution and transport of oxygen than using a foam flow field and a separate GDL. Foam materials that can be used as integrated GDL|FF include carbon-based foams and metal foams. Their respective advantages and disadvantages are described below.

Due to the acidic environment in which PEMFCs work, carbon-based porous materials exhibit better acid resistance and have little impact on proton conductors. Park *et al.* utilized graphene foam to replace the GDL and conventional flow field, as shown in Fig. 5g.[165] The graphene foam shortens the gas diffusion paths, allowing faster diffusion of reactants into the CL, and allows for easy removal of excess liquid water from the CL due to a high pressure drop. This configuration of the MEA significantly reduces the mass transfer resistance, allowing the fuel cell to operate at higher currents. As a result, compared with the conventional configuration, the volumetric power density of the PEMFC increased from 0.462 kW L^{-1} to 3.8 kW L^{-1} under their conditions. Nonetheless, there are some concerns about graphene foam as integrated GDL|FF. On the one hand, the graphene foam undergoes a large deformation with compression, and the porosity decreases significantly. On the other hand, the poor mechanical properties of graphene foam may make it difficult to support the catalyst layer and proton exchange membrane in the long term.

Compared with graphene foam, metallic foams have better mechanical properties, which can provide a better support for the CL and PEM, and the pore structure remains intact under compression. Moreover, the stability of metallic foams under acidic conditions can be solved by acid resistant coatings similar to the conventional metallic bipolar plate.[180–182] Therefore, metal foams may have better prospects as integrated GDL|FF. Chasen *et al.* reported an ultrathin GDL-less integrated electrode that replaced the GDL and the traditional flow field on the graphite plate with nickel foam.[166] To reduce the impact of nickel foam on the catalyst layer and proton exchange membrane under acidic conditions, they adopted a dual strategy: depositing a graphene coating and manufacturing a carbon nanofiber film as a protective layer. GDL-free integrated electrodes greatly reduce the volume of the MEA by 90% and shorten the transport paths of reactant gas by 96%. In a single PEMFC, GDL-free integrated electrodes achieved an ultra-high power density of up to 1.83 W cm^{-2} and 20.1 kW L^{-1}, which increased by 50% and 111% compared with the conventional configuration. Encouragingly, the authors evaluated a volumetric power density of 9.8 kW L^{-1} in a stack with GDL-free integrated electrodes, which represents an 80% increase over state-of-the-art commercial PEMFC stacks and attains the NEDO 2040 long-term target. Although metal foams have great potential in integrated GDL|FF, their rough and hard surface easily causes perforation of the membrane electrode. Ensuring the durability of the membrane electrode in long-term operation will be an important issue in promoting metal foams as integrated GDL|FF.

Although the above-mentioned integrated GDL|FF still have some issues to be resolved, they have great advantages in improving the volumetric power density of PEMFCs according to Fig. 5i.[164–168] In order to achieve a leap in the power density of PEMFCs in the future, it is not only important to improve the structure and performance of each component itself, but also necessary to optimize and redesign the structure of the entire PEMFC from the perspective of the stack as a whole. Integrated GDL|FF provides a new way of thinking on significantly improving the power density based on the overall structure of the PEMFC stack. This also raises the question of whether the structure of PEMFCs can be further integrated to maximize power density with the simplest structure.

6. Future trends and challenges of high-performance GDLs

We have extensively discussed various optimization methods for GDLs to achieve high-performance PEMFCs. Based on previous reports, we have systematically summarized multiple GDL design strategies and their corresponding performance metrics of PEMFCs fed with hydrogen and air, including peak power density and maximum current density with associated voltages, as presented in Table 1.

Currently, engineering the pore structure of GDLs, particularly in MPLs, represents the most prevalent strategy for structural optimization. This approach can be readily implemented using conventional MPL fabrication techniques such as spraying, blade coating, and screen printing, which are inherently scalable. However, it is important to note that the structural modifications achieved through these methods are typically incremental, making it challenging to fundamentally transform the morphology and distribution of GDL pores. Consequently, the resulting improvements in PEMFC performance are often limited. Engineering wettability faces similar constraints. As such, these methods may remain the primary approaches for GDL pore structure optimization in the near term. Additionally,

Table 1 The summary table of GDLs prepared by different design strategies and their corresponding performance metrics of PEMFCs

GDL	Design strategy	Maximum current density	Peak power density	Reference
Stacked MPL	Pore engineering	Approx. 2.03 A cm^{-2} @ 0.23 V	0.82 W cm^{-2}	183
GDL with gradient pores	Pore engineering	1.91 A cm^{-2} @ 0.2 V	0.83 W cm^{-2}	184
Gradient hydrophobic MPL	Pore engineering	Approx. 1.9 A cm^{-2} @ 0.4 V	0.86 W cm^{-2}	185
GDL with arrayed perforation	Pore engineering	Approx. 2.3 A cm^{-2} @ 0.32 V	0.92 W cm^{-2}	186
Buffer microporous layer	Pore engineering	Approx. 2.6 A cm^{-2} @ 0.32 V	1.02 W cm^{-2}	187
Grooved GDL	Pore engineering	2.28 A cm^{-2} @ 0.4 V	1.03 W cm^{-2}	188
Foam MPL	Pore engineering	Limiting 3.8 A cm^{-2}	1.10 W cm^{-2}	189
Carbon nanotube MPL	Pore engineering	Approx. 2.8 A cm^{-2} @ 0.2 V	1.18 W cm^{-2}	190
Cracked MPL	Pore engineering	Limiting 3.85 A cm^{-2}	1.21 W cm^{-2}	191
Porosity-graded MPL	Pore engineering	Approx. 2.6 A cm^{-2} @ 0.44 V	1.26 W cm^{-2}	192
Quadrilateral-patterned perforated GDL	Pore engineering	5.4 A cm^{-2} @ 0.2 V	1.43 W cm^{-2}	44
Patterned ZIF-8 hybrid MPL	Pore engineering	Approx. 4.5 A cm^{-2} @ 0.2 V	1.5 W cm^{-2}	120
Precisely tailored MPLs with 32 ± 5 nm hydrophobic pores	Pore engineering	Approx. 3.5 A cm^{-2} @ 0.41 V	1.57 W cm^{-2}	193
Ordered electrospun gas diffusion layer	Pore engineering	Limiting 7.2 A cm^{-2}	2.17 W cm^{-2}	194
Gas diffusion layer with hydrophobic and hydrophilic synergistic surfaces	Wettability engineering	Approx. 1.48 A cm^{-2} @ 0.37 V	0.59 W cm^{-2}	92
GDL with patterned wettability	Wettability engineering	Approx. 1.48 A cm^{-2} @ 0.37 V	0.64 W cm^{-2}	89
Patterned wettability GDL	Wettability engineering	Approx. 1.5 A cm^{-2} @ 0.35 V	0.68 W cm^{-2}	78
Three-dimensional graphene-Ni foam with patterned wettability	Wettability engineering	Approx. 2.34 A cm^{-2} @ 0.36V	0.92 W cm^{-2}	195
Microporous layer containing CeO$_2$-doped 3D graphene foam	Wettability engineering	Approx. 2.5 A cm^{-2} @ 0.32 V	1.01 W cm^{-2}	196
ZrO$_2$ hybrid GDL	Wettability engineering	Approx. 4 A cm^{-2} @ 0.25 V	1.36 W cm^{-2}	197
ZrO$_2$ hybrid MPL	Wettability engineering	3.35 A cm^{-2} @ 0.2 V	1.41 W cm^{-2}	198
Interfacial buffer layer	Wettability engineering	Approx. 3.4 A cm^{-2} @ 0.43 V	1.56 W cm^{-2}	149
Poly(1,5-diaminoanthraquinone)-modified gas diffusion backing	Wettability engineering	Approx. 3.6 A cm^{-2} @ 0.45 V	1.98 W cm^{-2}	199
Gas diffusion nanocomposite layer	Combining pore and wettability engineering	Approx. 1.75 A cm^{-2} @ 0.45 V	0.81 W cm^{-2}	200
MPL with carbon nanotubes	Combining pore and wettability engineering	Approx. 2.4 A cm^{-2} @ 0.49 V	1.18 W cm^{-2}	201
MPL with hydrophilic networks	Combining pore and wettability engineering	Approx. 2.6 A cm^{-2} @ 0.53 V	1.51 W cm^{-2}	202
Whole-root MPL	Combining pore and wettability engineering	5.37 A cm^{-2} @ 0.2 V	1.84 W cm^{-2}	107
Janus GDL	Combining pore and wettability engineering	5.19 A cm^{-2} @ 0.2 V	1.89 W cm^{-2}	82
GDL with ordered indentations	Interface optimization	Approx. 2.3 A cm^{-2} @ 0.34 V	0.87 W cm^{-2}	146
Surface controlled MPL	Interface optimization	Approx. 1.8 A cm^{-2} @ 0.54 V	0.98 W cm^{-2}	131
Wavy MPL	Interface optimization	Approx. 2.6 A cm^{-2} @ 0.42 V	1.14 W cm^{-2}	145
MPL with graphene	Interface optimization	Approx. 3.0 A cm^{-2} @ 0.4 V	Approx. 1.30 W cm^{-2}	203
Surface modified MPL	Interface optimization	Approx. 3.9 A cm^{-2} @ 0.14 V	1.30 W cm^{-2}	118
Standalone MPL	Interface optimization	2.94 A cm^{-2} @ 0.2 V	1.35 W cm^{-2}	116
GDL with gas-flow channels	Component integration	Approx. 3.0 A cm^{-2} @ 0.39 V	1.18 W cm^{-2}	169
Integrated GDL with flow field	Component integration	Approx. 3.3 A cm^{-2} @ 0.42 V	1.42 W cm^{-2}	164
Porous foam	Component integration	Approx. 4.4 A cm^{-2} @ 0.26 V	Approx. 1.48 W cm^{-2}	179
Integrated component with a flow field and GDL	Component integration	Approx. 3.3 A cm^{-2} @ 0.44 V	1.63 W cm^{-2}	167
3D flow field with a patterned GDL	Component integration	3.2 A cm^{-2} @ 0.52 V	1.70 W cm^{-2}	204
Graphene-coated Ni foam	Component integration	Approx. 5.5 A cm^{-2} @ 0.3 V	1.83 W cm^{-2}	166

the CL|GDL interface will likely be increasingly integrated with both GDL bulk modulation and CL optimization.

Regarding GDL bulk modulation, future research efforts will likely focus on two key aspects:

(1) Engineering of pore structure regularity: this involves the fabrication of GDLs with ordered pore architectures. For instance, Sun *et al.* recently developed a GDL with precisely controlled pore structures using electrospinning.[194]

(2) Combined engineering of pore structure and wettability: representative examples include the Janus GDL and root-inspired MPL we previously reported.[82,107] These advanced GDLs address critical challenges such as inefficient water transport

and the mutual interference between water and gas transport, significantly enhancing the efficiency of mass transport.

However, the materials and fabrication techniques for these innovative GDLs differ from conventional carbon paper-based approaches. While they deliver superior performance, their practical application necessitates robust durability and scalability. Thus, the following challenges must be addressed:

(1) Structural and wettability stability: the ordered pore structures must remain stable over prolonged operation without collapse or disordering. Similarly, wettability should either remain constant or stay within an acceptable range to minimize performance degradation.

(2) Scalability for mass production: the GDL must be compatible with commercially viable fabrication methods and possess sufficient mechanical strength to meet the standard dimensions of PEMFCs or enable roll-to-roll manufacturing.

(3) Cost-effectiveness: the production costs must be competitive to align with the industry's drive to reduce the expenses of PEMFCs.

The integrated GDL|FF design represents an emerging strategy with relatively low technological maturity in terms of fabrication and application. Due to its substantial modifications to the conventional PEMFC architecture and the limited validation of its operational stability and durability, this approach may remain in the R&D phase in the short term.

Nevertheless, existing studies have demonstrated that integrated GDL|FF designs not only achieve high power density (as shown in Table 1) but also simplify the PEMFC structure and reduce stack volume. Therefore, from a long-term perspective, integrated GDL|FF designs hold significant promise and may ultimately become the standard form of GDLs. However, before large-scale adoption, the following challenges must be overcome:

(1) Large-area, controllable fabrication: the primary hurdle lies in the fabrication process. Given the thinness of the GDL and the precision required for flow field dimensions, achieving large-area, batch production with precise structural control remains a major challenge.

(2) Stability and durability: current integrated GDL|FF designs lack comprehensive validation of their long-term stability. For carbon paper with flow fields or porous carbon/metal foams, the porous ridge structures must maintain mechanical integrity under prolonged operation to prevent damage from gas and water flow. For metal foams, corrosion resistance is also critical. Additionally, potential impacts on other components, such as membrane poisoning from metal leaching or mechanical aging from carbon fibers, must be carefully evaluated.

(3) Cost-effectiveness: the production costs must be justified to meet the industry's cost-reduction targets.

Beyond these specific challenges, GDL design and optimization face broader obstacles:

(1) Theoretical foundations: a deeper understanding of gas and water transport mechanisms in GDLs and their relationship with PEMFC performance is needed. Advanced theories and visualization techniques could provide critical insights to guide the design of GDLs.

(2) Broad and simple operating conditions: future GDL optimization must deliver high performance under low stoichiometric ratios, low backpressure, and wide humidity ranges—especially under low humidity—to simplify balance-of-plant systems and reduce their energy consumption.

(3) System-level coordination: GDL structural design must be better coordinated with other fuel cell components. The integrated GDL|FF concept serves as an excellent example, inspiring future innovations that combine GDLs with CLs, flow fields, and other elements to develop highly integrated, unified electrodes.

(4) Artificial intelligence-driven design: current GDL optimization largely relies on trial-and-error methods, which are inefficient and yield low success rates. A recent report by Sun *et al.* demonstrated the potential of Bayesian machine learning to guide GDL pore structure design, resulting in state-of-the-art ordered-pore GDLs.[194] This highlights the transformative potential of artificial intelligence in accelerating and optimizing GDL development.

In summary, while significant progress has been made in GDL optimization, addressing these challenges will be crucial for advancing PEMFC technology toward higher performance, durability, and commercial viability.

7. Summary and outlook

Currently, research and development efforts on GDLs predominantly concentrate on structural engineering aspects, particularly pore architecture, wettability control, and interface optimization. While the integrated GDL|FF configuration has shown considerable promise, its practical implementation remains at a nascent stage, necessitating comprehensive validation regarding manufacturing costs and long-term durability. Consequently, PEMFCs are expected to maintain their conventional architecture (Fig. 1a) in the near future. Nevertheless, with continuous advancements in CL and catalyst-coated membrane fabrication technologies, addressing critical mass transport challenges within GDLs becomes imperative for achieving superior power density. Based on these considerations, we propose the following strategic roadmap for future GDL development:

(1) Near-term focus: carbon paper substrates incorporating MPLs will remain the mainstream GDL configuration. Primary research efforts should continue to optimize pore structure engineering, wettability tuning, and CL|GDL interface modification, as these approaches offer practical scalability and manufacturing feasibility.

(2) Medium-term development: the synergistic combination of pore structure engineering, wettability control and the implementation of ordered pore architectures will emerge as crucial research directions. These strategies promise enhanced mass transport efficiency while presenting manageable challenges for industrial-scale production.

(3) Long-term vision: integrated GDL|FF and other innovative component integration approaches represent transformative research frontiers. However, their commercialization will require extensive development efforts to overcome challenges related to cost-effective mass production, durability

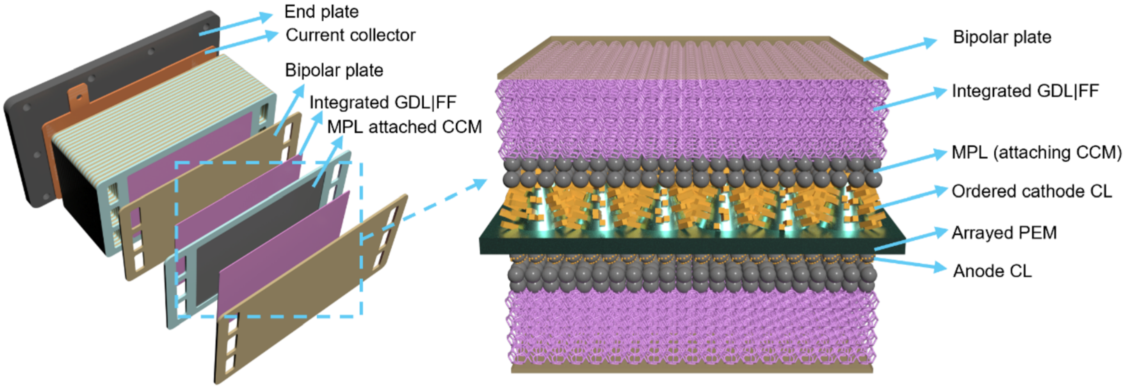

Fig. 6 Scheme of an optimal and highly integrated PEMFC stack.

validation, and system reliability, given their fundamentally disruptive nature to conventional fuel cell design paradigms.

Although current CCMs already enable operating currents to be higher than 2 A cm^{-2}, next-generation ordered MEAs, such as patterned PEMs and ordered CLs, are gaining traction, offering distinct advantages in enhancing catalyst utilization and the three-phase interfaces within electrodes.[205–208] These advancements contribute to reducing the precious metal catalyst loading and lowering the overall cost of PEMFCs. However, the very thin CL places very high gas and water transport requirements on the ordered MEA. Most of the past studies focused on ordered PEMs or ordered CLs but neglected the effect of the bulk GDL and the CL|GDL interface on the performance of PEMFCs, which play an important role in improving performance of these ordered structures. As previously reported, Jia demonstrated improved water management in nanostructured thin film cathode electrodes, an ordered CL prone to be flooded developed by 3M company, by using GDLs with patterned wettability.[93] In the future, designing PEMFCs with ordered MEAs will require greater attention to optimizing GDLs in facilitating water and gas transport, while also enhancing the CL|GDL interface to ensure efficient electron conduction and mass transfer.

Further, the design of the ultimate PEMFC requires a redesign of the components to simplify the structure of a single unit and minimize the stack size while increasing the power density. The integrated GDL|FF represents a breakthrough in structural design, which not only realizes the enhancement of water and gas transport in the MEA but also simplifies the PEMFC structure and reduces its volume. Therefore, although the traditional PEMFC structure still represents the mainstream for some time to come, the integrated GDL|FF is very promising for rapid development and eventual commercialization. Most importantly, the integrated design of GDL|FF provides a novel perspective on PEMFC architecture, paving the way for deeper integration of advanced components that has huge potential to achieve unprecedented power density increases while significantly reducing costs.

At the end, we propose an optimal and highly integrated PEMFC stack, as shown in Fig. 6, from the perspective of fuel cell architectures and their latest research advances. Ordered CLs are grown onto arrayed PEMs, and perfect CL|MPL interfaces are constructed using MPL-attached CCMs. Metallic foams are used as integrated GDL|FFs, and bipolar plates are made of only ultra-thin hollow metal plates.

Conflicts of interest

There are no conflicts to declare.

Data availability

This perspective article does not present any new data generated by the authors. All data discussed in this review are derived from previously published studies, which are cited accordingly within the text. No additional data are available.

Acknowledgements

The authors are grateful for financial support granted by the National Natural Science Foundation of China (No. 22172191) and CAS H2 Technology (Suzhou) Co., Ltd (E341150301).

References

1 Z. P. Cano, D. Banham, S. Ye, A. Hintennach, J. Lu, M. Fowler and Z. Chen, *Nat. Energy*, 2018, **3**, 279–289.
2 D. A. Cullen, K. C. Neyerlin, R. K. Ahluwalia, R. Mukundan, K. L. More, R. L. Borup, A. Z. Weber, D. J. Myers and A. Kusoglu, *Nat. Energy*, 2021, **6**, 462–474.
3 M. A. Aminudin, S. K. Kamarudin, B. H. Lim, E. H. Majilan, M. S. Masdar and N. Shaari, *Int. J. Hydrogen Energy*, 2023, **48**, 4371–4388.
4 T. Takahashi, T. Ikeda, K. Murata, O. Hotaka, S. Hasegawa, Y. Tachikawa, M. Nishihara, J. Matsuda, T. Kitahara and S. M. Lyth, *J. Electrochem. Soc.*, 2022, **169**, 044523.
5 T. Takahashi, Y. Kokubo, K. Murata, O. Hotaka, S. Hasegawa, Y. Tachikawa, M. Nishihara, J. Matsuda, T. Kitahara, S. M. Lyth, A. Hayashi and K. Sasaki, *Int. J. Hydrogen Energy*, 2022, **47**, 41111–41123.

6 K. Jiao, J. Xuan, Q. Du, Z. Bao, B. Xie, B. Wang, Y. Zhao, L. Fan, H. Wang, Z. Hou, S. Huo, N. P. Brandon, Y. Yin and M. D. Guiver, *Nature*, 2021, **595**, 361–369.

7 T. Suzuki, A. Iiyama, N. Kubo, N. Saito, K. Shinohara, S. Shimotori, Y. Sugawara and K. Yamada, *ECS Trans.*, 2019, **92**, 3.

8 R. O'Hayre, S.-W. Cha, W. Colella and F. B. Prinz, in *Fuel Cell Fundamentals*, John Wiley & Sons, Inc., Hoboken, 3rd edn, 2016, chapter 1: introduction, pp. 1–24.

9 X. Huang, Z. Zhang and J. Jiang, in *2006 IEEE International Symposium on Industrial Electronics, IEEE Montreal, Year, Fuel Cell Technology for Distributed Generation: an Overview*, pp. , pp. 1613–1618.

10 M. Han, J. H. Xu, S. H. Chan and S. P. Jiang, *Electrochim. Acta*, 2008, **53**, 5361–5367.

11 D. Ye, E. Gauthier, J. B. Benziger and M. Pan, *J. Power Sources*, 2014, **256**, 449–456.

12 I. Nitta, O. Himanen and M. Mikkola, *Electrochem. Commun.*, 2008, **10**, 47–51.

13 S. Park and B. N. Popov, *Fuel*, 2009, **88**, 2068–2073.

14 F. C. Lee, M. S. Ismail, D. B. Ingham, K. J. Hughes, L. Ma, S. M. Lyth and M. Pourkashanian, *Renewable Sustainable Energy Rev.*, 2022, **166**, 112640.

15 M. A. A. Hamzah, S. K. Kamarudin, M. Beygisangchin, N. Shaari, R. Hazan and Z. Zakaria, *J. Environ. Chem. Eng.*, 2024, **12**, 114220.

16 Y. Wang, C.-Y. Wang and K. S. Chen, *Electrochim. Acta*, 2007, **52**, 3965–3975.

17 M. Mortazavi and K. Tajiri, *Int. J. Hydrogen Energy*, 2014, **39**, 9409–9419.

18 M. Chen, C. Zhao, F. Sun, J. Fan, H. Li and H. Wang, *eTransportation*, 2020, **5**, 100075.

19 Z. Shangguan, B. Li, P. Ming and C. Zhang, *J. Mater. Chem. A*, 2021, **9**, 15111–15139.

20 S. Deng and Y. Li, *Energy Convers. Manage.*, 2022, **263**, 115707.

21 Z. Jiang, G. Yang, Q. Shen, S. Li, J. Liao, X. Yang and J. Sun, *Mater. Today Commun.*, 2023, **37**, 107633.

22 G. Karimi, X. Li and P. Teertstra, *Electrochim. Acta*, 2010, **55**, 1619–1625.

23 S. Litster, D. Sinton and N. Djilali, *J. Power Sources*, 2006, **154**, 95–105.

24 D. Niblett, V. Niasar and S. Holmes, *J. Electrochem. Soc.*, 2020, **167**, 013520.

25 D. Niblett, Z. Guo, S. Holmes, V. Niasar and R. Prosser, *Int. J. Hydrogen Energy*, 2022, **47**, 23393–23410.

26 T. Gu, R. Shi, J. Guo, W. Wang, X. Wei, Q. Zhang, J. Luo and R. Yang, *Energy Fuels*, 2024, **38**, 15714–15720.

27 X. Wang, H. Ma, H. Peng, Y. Wang, G. Wang, L. Xiao, J. Lu and L. Zhuang, *J. Power Sources*, 2021, **515**, 230636.

28 B. Huang, X. Wang, W. Li, W. Tian, L. Luo, X. Sun, G. Wang, L. Zhuang and L. Xiao, *Angew. Chem., Int. Ed.*, 2023, **62**, e202304230.

29 B. Huang, C. Lei, X. Sun, L. Luo, G. Wang, L. Zhuang and L. Xiao, *Int. J. Hydrogen Energy*, 2023, **48**, 35453–35462.

30 C. Geiger, J. Kriegler, T. Weiss, A. Berger and M. F. Zaeh, *Procedia CIRP*, 2022, **111**, 796–799.

31 C. Csoklich, T. J. Schmidt and F. N. Büchi, *Energy Environ. Sci.*, 2022, **15**, 1293–1306.

32 I. Bae, B. Kim, D.-Y. Kim, H. Kim and K.-H. Oh, *Renewable Energy*, 2020, **146**, 960–967.

33 H. Tang, S. Wang, M. Pan and R. Yuan, *J. Power Sources*, 2007, **166**, 41–46.

34 M. Balakrishnan, P. Shrestha, N. Ge, C. Lee, K. F. Fahy, R. Zeis, V. P. Schulz, B. D. Hatton and A. Bazylak, *ACS Appl. Energy Mater.*, 2020, **3**, 2695–2707.

35 X. Wang and G.-P. Wu, *ACS Sustainable Chem. Eng.*, 2024, **12**, 6596–6605.

36 K. Narita, M. A. Citrin, H. Yang, X. Xia and J. R. Greer, *Adv. Energy Mater.*, 2021, **11**, 2002637.

37 F.-Y. Zhang, S. G. Advani and A. K. Prasad, *J. Power Sources*, 2008, **176**, 293–298.

38 S. Tanaka and A. G. Malan, *J. Power Sources*, 2019, **413**, 198–208.

39 S. Tanaka, W. W. Bradfield, C. Legrand and A. G. Malan, *J. Power Sources*, 2016, **330**, 273–284.

40 J. Benziger, J. Nehlsen, D. Blackwell, T. Brennan and J. Itescu, *J. Membr. Sci.*, 2005, **261**, 98–106.

41 A. Mohseninia, D. Kartouzian, M. Eppler, P. Langner, H. Markötter, F. Wilhelm, J. Scholta and I. Manke, *Fuel Cells*, 2020, **20**, 469–476.

42 D. Gerteisen, T. Heilmann and C. Ziegler, *J. Power Sources*, 2008, **177**, 348–354.

43 Z. Bao, Y. Li, X. Zhou, F. Gao, Q. Du and K. Jiao, *Int. J. Heat Mass Transfer*, 2021, **178**, 121608.

44 P. Lin, J. Sun, C. He, M. Wu and T. Zhao, *ACS Energy Lett.*, 2024, **9**, 1710–1716.

45 D. Gerteisen and C. Sadeler, *J. Power Sources*, 2010, **195**, 5252–5257.

46 C. Csoklich, H. Xu, F. Marone, T. J. Schmidt and F. N. Büchi, *ACS Appl. Energy Mater.*, 2021, **4**, 12808–12818.

47 S. M. Mahnama and M. Khayat, *J. Renewable Sustainable Energy*, 2017, **9**, 014301.

48 J. Lee, R. Yip, P. Antonacci, N. Ge, T. Kotaka, Y. Tabuchi and A. Bazylak, *J. Electrochem. Soc.*, 2015, **162**, F669–F676.

49 Y. Nagai, J. Eller, T. Hatanaka, S. Yamaguchi, S. Kato, A. Kato, F. Marone, H. Xu and F. N. Büchi, *J. Power Sources*, 2019, **435**, 226809.

50 Z. Lu, M. M. Daino, C. Rath and S. G. Kandlikar, *Int. J. Hydrogen Energy*, 2010, **35**, 4222–4233.

51 T. Sasabe, P. Deevanhxay, S. Tsushima and S. Hirai, *Electrochem. Commun.*, 2011, **13**, 638–641.

52 R. Shi, Q. Zhang, T. Gu, J. Guo, X. Wang, W. Wang, X. Wei, W. Xing, H. Wang and R. Yang, *ACS Sustainable Chem. Eng.*, 2023, **11**, 3944–3951.

53 X. Shi, D. Jiao, Z. Bao, K. Jiao, W. Chen and Z. Liu, *Int. J. Hydrogen Energy*, 2022, **47**, 6247–6258.

54 H. Markötter, J. Haußmann, R. Alink, C. Tötzke, T. Arlt, M. Klages, H. Riesemeier, J. Scholta, D. Gerteisen, J. Banhart and I. Manke, *Electrochem. Commun.*, 2013, **34**, 22–24.

55 Y. Yu, S. Chen and H. Wei, *Int. J. Heat Mass Transfer*, 2023, **212**, 124275.

56 D. Niblett, V. Niasar, S. Holmes, A. Mularczyk, J. Eller, R. Prosser and M. Mamlouk, *J. Power Sources*, 2023, **555**, 232383.

57 Z. Chen, W. Pan, D. Yao, M. Gao, Y. Gao, X. Chen, J. Krzywanski and F. Wang, *Colloids Surf., A*, 2022, **650**, 129283.

58 C. S. Kong, D.-Y. Kim, H.-K. Lee, Y.-G. Shul and T.-H. Lee, *J. Power Sources*, 2002, **108**, 185–191.

59 T. Li, K. Wang, J. Wang, Y. Liu, Y. Han, J. Song, H. Hu, G. Lin and Y. Liu, *J. Mater. Sci.*, 2020, **55**, 4558–4569.

60 L. Chen, R. Lin, X. Chen, Z. Hao, X. Diao, D. Froning and S. Tang, *ACS Appl. Mater. Interfaces*, 2020, **12**, 24048–24058.

61 C. Simon, D. Kartouzian, D. Müller, F. Wilhelm and H. A. Gasteiger, *J. Electrochem. Soc.*, 2017, **164**, F1697–F1711.

62 W. Li, Q. Wen, F. Ning, X. Dan, C. He, Y. Li, S. Pan and X. Zhou, *Energy Technol.*, 2023, **11**, 2201485.

63 Z. Lu, J. Waldecker, X. Xie, M.-C. Lai, D. S. Hussey and D. L. Jacobson, *ECS Trans.*, 2013, **58**, 315.

64 Y. Hiramitsu, K. Kobayashi and M. Hori, *J. Power Sources*, 2010, **195**, 7559–7567.

65 H. Oh, J. Park, K. Min, E. Lee and J.-Y. Jyoung, *Appl. Energy*, 2015, **149**, 186–193.

66 C. Li, D. Si, Y. Liu, J. Zhang and Y. Liu, *Int. J. Hydrogen Energy*, 2021, **46**, 11150–11159.

67 G. Ren, Z. Qu, X. Wang, G. Zhang and Y. Wang, *Int. J. Hydrogen Energy*, 2024, **55**, 455–463.

68 Q. Duan, B. Wang, J. Wang, H. Wang and Y. Lu, *J. Power Sources*, 2010, **195**, 8189–8193.

69 J. Guo, W. Wang, R. Shi, T. Gu, X. Wei, J. Zhao, M. Chao, Q. Zhang and R. Yang, *J. Mater. Sci.*, 2024, **59**, 3561–3572.

70 G. Lin, S. Liu, B. Yu, H. Wang, K. Yu and Y. Hu, *J. Appl. Polym. Sci.*, 2020, **137**, 49564.

71 T. Li, G. Chen and G. Lin, *Ceram. Int.*, 2023, **49**, 20715–20722.

72 A. Forner-Cuenca, J. Biesdorf, L. Gubler, P. M. Kristiansen, T. J. Schmidt and P. Boillat, *Adv. Mater.*, 2015, **27**, 6317–6322.

73 S. G. Kandlikar, M. L. Garofalo and Z. Lu, *Fuel Cells*, 2011, **11**, 814–823.

74 M. Afra, M. Nazari, M. H. Kayhani, M. Sharifpur and J. P. Meyer, *Energy*, 2019, **175**, 967–977.

75 A. Li, M. Han, S. H. Chan and N.-t. Nguyen, *Electrochim. Acta*, 2010, **55**, 2706–2711.

76 G. S. Avcioglu, B. Ficicilar and I. Eroglu, *Int. J. Hydrogen Energy*, 2018, **43**, 18632–18641.

77 Y. Li and T. Van Nguyen, *J. Electrochem. Soc.*, 2022, **169**, 114505.

78 W. Zhang, F. Guo, Y. Zhou, S. Yu, A. Chen, H. Jiang, H. Jiang and C. Li, *ACS Appl. Mater. Interfaces*, 2022, **14**, 17578–17584.

79 T. Kitahara, H. Nakajima, M. Inamoto and K. Shinto, *J. Power Sources*, 2014, **248**, 1256–1263.

80 X. Li, R. Liu, M. Yao, J. Zhang and Y. Liu, *J. Power Sources*, 2022, **545**, 231896.

81 M. N. Islam, U. Shrivastava, M. Atwa, X. Li, V. Birss and K. Karan, *ACS Appl. Mater. Interfaces*, 2020, **12**, 39215–39226.

82 Q. Wen, S. Pan, Y. Li, C. Bai, M. Shen, H. Jin, F. Ning, X. Fu and X. Zhou, *ACS Energy Lett.*, 2022, **7**, 3900–3909.

83 A. Forner-Cuenca, V. Manzi-Orezzoli, J. Biesdorf, M. E. Kazzi, D. Streich, L. Gubler, T. J. Schmidt and P. Boillat, *J. Electrochem. Soc.*, 2016, **163**, F788–F801.

84 A. Forner-Cuenca, J. Biesdorf, A. Lamibrac, V. Manzi-Orezzoli, F. N. Büchi, L. Gubler, T. J. Schmidt and P. Boillat, *J. Electrochem. Soc.*, 2016, **163**, F1038–F1048.

85 A. Forner-Cuenca, J. Biesdorf, V. Manzi-Orezzoli, L. Gubler, T. J. Schmidt and P. Boillat, *J. Electrochem. Soc.*, 2016, **163**, F1389–F1398.

86 Z. Zhang, M. Guo, Z. Yu, S. Yao, J. Wang, D. Qiu and L. Peng, *Energy*, 2022, **239**, 122375.

87 R. Kaneko, V. Chate and K. Nishida, *ECS Trans.*, 2023, **112**, 63–68.

88 R. Koresawa and Y. Utaka, *J. Power Sources*, 2014, **271**, 16–24.

89 F. Calili-Cankir, E. M. Can, D. B. Ingham, K. J. Hughes, L. Ma, M. Pourkashanian, S. M. Lyth and M. S. Ismail, *Chem. Eng. J.*, 2024, **484**, 149711.

90 A. Lim, H.-Y. Jeong, Y. Lim, J. Y. Kim, H. Y. Park, J. H. Jang, Y.-E. Sung, J. M. Kim and H. S. Park, *Sci. Adv.*, 2021, **7**, eabf7866.

91 G. Wang, Y. Utaka and S. Wang, *J. Power Sources*, 2019, **437**, 226930.

92 F. Guo, X. Yang, H. Jiang, Y. Zhu and C. Li, *J. Power Sources*, 2020, **451**, 227784.

93 J. Jia, X. Liu, F. Liu, H. Yin and Y. Ding, *Int. J. Hydrogen Energy*, 2022, **47**, 21261–21272.

94 G. Wang, Y. Utaka and S. Wang, *Energies*, 2020, **13**, 3529.

95 R. Schweiss, M. Steeb and P. M. Wilde, *Fuel Cells*, 2010, **10**, 1176–1180.

96 D. Spernjak, R. Mukundan, R. L. Borup, L. G. Connolly, B. I. Zackin, V. De Andrade, M. Wojcik, D. Y. Parkinson, D. L. Jacobson, D. S. Hussey, K. L. More, T. Chan, A. Z. Weber and I. V. Zenyuk, *ACS Appl. Energy Mater.*, 2018, **1**, 6006–6017.

97 Y. Wang, L. Wang, S. G. Advani and A. K. Prasad, *J. Power Sources*, 2015, **292**, 39–48.

98 I. M. Kong, A. Jung, Y. S. Kim and M. S. Kim, *Energy*, 2017, **120**, 478–487.

99 J. H. Chun, K. T. Park, D. H. Jo, J. Y. Lee, S. G. Kim, S. H. Park, E. S. Lee, J.-Y. Jyoung and S. H. Kim, *Int. J. Hydrogen Energy*, 2011, **36**, 8422–8428.

100 T. Kitahara, H. Nakajima and K. Mori, *J. Power Sources*, 2012, **199**, 29–36.

101 T. Kitahara and H. Nakajima, *Int. J. Hydrogen Energy*, 2016, **41**, 9547–9555.

102 F.-B. Weng, C.-Y. Hsu and M.-C. Su, *Int. J. Hydrogen Energy*, 2011, **36**, 13708–13714.

103 P. Shrestha, D. Ouellette, J. Lee, N. Ge, A. K. C. Wong, D. Muirhead, H. Liu, R. Banerjee and A. Bazylak, *Adv. Mater. Interfaces*, 2019, **6**, 1901157.

104 G. Lin, S. Liu, S. Qu, G. Qu, L. Tianya, Z. Liang, Y. Hu and F. Liu, *J. Appl. Polym. Sci.*, 2020, **138**, 50355.

105 P. Wang, H. Nakajima and T. Kitahara, *J. Electrochem. Soc.*, 2023, **170**, 124514.

106 T. Kitahara, H. Nakajima, M. Inamoto and M. Morishita, *J. Power Sources*, 2013, **234**, 129–138.

107 Q. Wen, C. He, F. Ning, M. Shen, Y. Liu, Z. Chai, X. Cheng, X. Dan, S. Zou, W. Li, L. He, B. Tian and X. Zhou, *Chem. Eng. J.*, 2024, **497**, 154424.

108 N. B. Carrigy, L. M. Pant, S. Mitra and M. Secanell, *J. Electrochem. Soc.*, 2012, **160**, F81–F89.

109 J. Zhou, S. Shukla, A. Putz and M. Secanell, *Electrochim. Acta*, 2018, **268**, 366–382.

110 F. Lapicque, M. Belhadj, C. Bonnet, J. Pauchet and Y. Thomas, *J. Power Sources*, 2016, **336**, 40–53.

111 L. Castanheira, M. Bedouet, A. Kucernak and G. Hinds, *J. Power Sources*, 2019, **418**, 147–151.

112 Y. Tabe, Y. Aoyama, K. Kadowaki, K. Suzuki and T. Chikahisa, *J. Power Sources*, 2015, **287**, 422–430.

113 T. Swamy, E. C. Kumbur and M. M. Mench, *J. Electrochem. Soc.*, 2010, **157**, B77–B85.

114 C. Hartnig, I. Manke, R. Kuhn, N. Kardjilov, J. Banhart and W. Lehnert, *Appl. Phys. Lett.*, 2008, **92**, 134106.

115 M. Wang, S. Medina, J. R. Pfeilsticker, S. Pylypenko, M. Ulsh and S. A. Mauger, *ACS Appl. Energy Mater.*, 2019, **2**, 7757–7761.

116 Q. Wen, Y. Li, C. He, M. Shen, F. Ning, X. Dan, Y. Liu, P. Xu, S. Zou and Z. Chai, *Adv. Mater.*, 2023, **35**, 2301504.

117 L. Daniel, A. Bonakdarpour, J. Sharman and D. P. Wilkinson, *Fuel Cells*, 2020, **20**, 224–228.

118 R. Lin, X. Yu, L. Chen, S. Tang, X. Yin and Z. Hao, *Energy Convers. Manage.*, 2021, **243**, 114319.

119 J. Iglesia, C.-C. Lang, Y.-M. Chen, S.-y. Chen and C.-J. Tseng, *J. Power Sources*, 2019, **436**, 226886.

120 L. Wang, J. Yao, Y. Pei, W. Zhu, Z. Che, J. Zhang, Y. Yin and M. D. Guiver, *J. Power Sources*, 2024, **616**, 235136.

121 J. H. Nam, K.-J. Lee, G.-S. Hwang, C.-J. Kim and M. Kaviany, *Int. J. Heat Mass Transfer*, 2009, **52**, 2779–2791.

122 P. Deevanhxay, T. Sasabe, S. Tsushima and S. Hirai, *Electrochem. Commun.*, 2013, **34**, 239–241.

123 H. Bajpai, M. Khandelwal, E. C. Kumbur and M. M. Mench, *J. Power Sources*, 2010, **195**, 4196–4205.

124 Z. Chen, W. Pan, L. Tang, X. Chen and F. Wang, *Fuel*, 2024, **360**, 130629.

125 Z. Chen, W. Pan, L. Tang, X. Chen and F. Wang, *Chin. J. Chem. Eng.*, 2024, **69**, 1–12.

126 S. Prass, S. Hasanpour, P. K. Sow, A. B. Phillion and W. Mérida, *J. Power Sources*, 2016, **319**, 82–89.

127 F. E. Hizir, S. O. Ural, E. C. Kumbur and M. M. Mench, *J. Power Sources*, 2010, **195**, 3463–3471.

128 J. H. Chun, D. H. Jo, S. G. Kim, S. H. Park, C. H. Lee and S. H. Kim, *Renewable Energy*, 2012, **48**, 35–41.

129 D. Ramani, N. S. Khattra, Y. Singh, A. Mohseni-Javid, F. P. Orfino, M. Dutta and E. Kjeang, *J. Power Sources*, 2021, **512**, 230446.

130 C. H. Chen, K. Khedekar, A. Zaffora, M. Santamaria, M. Coats, S. Pylypenko, P. A. García-Salaberri, J. Braaten, P. Atanassov, N. Tamura, C. Johnston, L. Cheng and I. V. Zenyuk, *ACS Appl. Energy Mater.*, 2024, **7**, 5736–5744.

131 G. Li, T. Xu, S. Luo, Q. Wang, X. Li, D. Xing, P. Ming, B. Li and C. Zhang, *J. Power Sources*, 2024, **623**, 235415.

132 S. Du, B. Millington and B. G. Pollet, *Int. J. Hydrogen Energy*, 2011, **36**, 4386–4393.

133 Y. Xing, L. Liu, Z. Fu, Y. Li and H. Li, *Energy Fuels*, 2023, **37**, 12360–12368.

134 K. Qiao, H. Liu, K. Ren, P. Sun, L. Yang, S. Wang and D. Cao, *Sustainable Energy Fuels*, 2023, **7**, 1829–1838.

135 M. Klingele, M. Breitwieser, R. Zengerle and S. Thiele, *J. Mater. Chem. A*, 2015, **3**, 11239–11245.

136 H. Ito, Y. Heo, M. Ishida, A. Nakano, S. Someya and T. Munakata, *J. Power Sources*, 2017, **342**, 393–404.

137 D. Joo, S. M. Jin, J. H. Jang and S. Park, *Fuel Cells*, 2018, **18**, 57–62.

138 J. Kim, H. Kim, H. Song, D. Kim, G. H. Kim, D. Im, Y. Jeong and T. Park, *Energy*, 2021, **227**, 120459.

139 J. Kim, O. Kwon, H. Yoo, H. Choi, H. Cha, H. Kim, S. Jeong, M. Shin, D. Im, Y. Jeong and T. Park, *J. Power Sources*, 2022, **537**, 231416.

140 D. Ebenezer, K. Neelima, M. Jagannatham and P. Haridoss, *Fuel Cells*, 2016, **16**, 349–355.

141 X. Fu, J. Wei, F. Ning, C. Bai, Q. Wen, H. Jin, Y. Li, S. Zou, S. Pan, J. Chen, S. Deng and X. Zhou, *J. Power Sources*, 2022, **520**, 230832.

142 J. Park, U. Pasaogullari and L. J. Bonville, *ECS Trans.*, 2015, **69**, 1355.

143 T. Tanuma, *ECS Trans.*, 2017, **80**, 165.

144 D.-H. Lee, M. K. Kim, H. Guim, S. Yuk, J. Choi, S. Choi, G. Doo, D. W. Lee, J. Noh and H.-T. Kim, *Mater. Adv.*, 2020, **1**, 254–261.

145 L. Chen, R. Lin, M. Lou and K. Lu, *Carbon*, 2022, **199**, 189–199.

146 L. Chen, R. Lin, M. Dong, X. Yu, M. Lou and Z. Hao, *J. Phys. Chem. C*, 2021, **125**, 14122–14133.

147 S. Wang, K. Hu, W. Chen, Y. Cao, L. Wang, Z. Wang, L. Cui, M. Zhou, W. Zhu and H. Li, *Nano Res.*, 2024, 1–7.

148 J. Cho, S. Lee, B. S. Shim, S. Y. Jung, D. Kim and S. Park, *J. Power Sources*, 2021, **491**, 229563.

149 L. Chen and R. Lin, *J. Phys. Chem. C*, 2024, **128**, 12879–12890.

150 H. Wang, R. Lin, X. Liu, S. Liu, X. Cai and W. Ji, *ACS Appl. Mater. Interfaces*, 2022, **14**, 27891–27901.

151 A. Kusoglu and A. Z. Weber, *Chem. Rev.*, 2017, **117**, 987–1104.

152 F. A. de Bruijn, V. A. T. Dam and G. J. M. Janssen, *Fuel Cells*, 2008, **8**, 3–22.

153 X. X. Wang, M. T. Swihart and G. Wu, *Nat. Catal.*, 2019, **2**, 578–589.

154 A. Pedersen, A. Bagger, J. Barrio, F. Maillard, I. E. L. Stephens and M.-M. Titirici, *J. Mater. Chem. A*, 2023, **11**, 23211–23222.

155 F. Ning, C. Bai, J. Qin, Y. Song, T. Zhang, J. Chen, J. Wei, G. Lu, H. Wang and Y. Li, *J. Mater. Chem. A*, 2020, **8**, 5489–5500.

156 B. Yang and Z. Xiang, *ACS Nano*, 2024, **18**, 11598–11630.

157 W. Huang, Y. Jiang, F. Ning, Y. Liu, Q. Wen, W. Li, A. Hammad, L. He, X. Zhu, X. Dan, X. Cheng, S. Zou, D. Yang, P. Cao, B. Tian and X. Zhou, *Adv. Funct. Mater.*, 2025, e08864.

158 S. Porstmann, T. Wannemacher and W. G. Drossel, *J. Manuf. Process.*, 2020, **60**, 366–383.

159 J. Zhang, D. Kramer, R. Shimoi, Y. Ono, E. Lehmann, A. Wokaun, K. Shinohara and G. G. Scherer, *Electrochim. Acta*, 2006, **51**, 2715–2727.

160 S. S. Alrwashdeh, I. Manke, H. Markötter, M. Klages, M. Göbel, J. Haußmann, J. Scholta and J. Banhart, *ACS Nano*, 2017, **11**, 5944–5949.

161 M. Siegwart, V. Manzi-Orezzoli, J. Valsecchi, R. P. Harti, M. Kagias, M. Strobl, C. Grünzweig, T. J. Schmidt and P. Boillat, *J. Electrochem. Soc.*, 2020, **167**, 064509.

162 T. Inoue, D. Sakai, K. Hirota, K. Sano, M. Nasu, H. Yanai, M. Watanabe, A. Iiyama and M. Uchida, *J. Electrochem. Soc.*, 2022, **169**, 114504.

163 M. Nasu, H. Yanai, N. Hirayama, H. Adachi, Y. Kakizawa, Y. Shirase, H. Nishiyama, T. Kawamoto, J. Inukai, T. Shinohara, H. Hayashida and M. Watanabe, *J. Power Sources*, 2022, **530**, 231251.

164 C. He, Q. Wen, F. Ning, M. Shen, L. He, Y. Li, B. Tian, S. Pan, X. Dan and W. Li, *Adv. Sci.*, 2023, **10**, 2302928.

165 J. E. Park, J. Lim, M. S. Lim, S. Kim, O.-H. Kim, D. W. Lee, J. H. Lee, Y.-H. Cho and Y.-E. Sung, *Electrochim. Acta*, 2019, **323**, 134808.

166 C. Tongsh, S. Wu, K. Jiao, W. Huo, Q. Du, J. W. Park, J. Xuan, H. Wang, N. P. Brandon and M. D. Guiver, *Joule*, 2024, **8**, 175–192.

167 C. He, Q. Wen, F. Ning, M. Shen, L. He, B. Tian, W. Li, L. Xu, Y. Liu and X. Dan, *Adv. Funct. Mater.*, 2024, 2401261.

168 G. Zhang, L. Wu, C. Tongsh, Z. Qu, S. Wu, B. Xie, W. Huo, Q. Du, H. Wang and L. An, *Small Methods*, 2023, **7**, 2201537.

169 M. Watanabe, H. Yanai and M. Nasu, *J. Electrochem. Soc.*, 2019, **166**, F3210–F3215.

170 T. Inoue, D. Sakai, N. Hirayama, M. Nasu, T. Suzuki, S. Tsushima, J. Inukai, D. A. Tryk, M. Watanabe and A. Iiyama, *J. Power Sources*, 2023, **585**, 233623.

171 M. A. Müller, C. Müller, R. Förster and W. Menz, *Microsyst. Technol.*, 2005, **11**, 280–281.

172 C.-J. Tseng, B. T. Tsai, Z.-S. Liu, T.-C. Cheng, W.-C. Chang and S.-K. Lo, *Energy Convers. Manage.*, 2012, **62**, 14–21.

173 Z. Bao, Z. Niu and K. Jiao, *Appl. Energy*, 2020, **280**, 116011.

174 M. Kim, C. Kim and Y. Sohn, *Fuel Cells*, 2018, **18**, 123–128.

175 H. Choi, O.-H. Kim, M. Kim, H. Choe, Y.-H. Cho and Y.-E. Sung, *ACS Appl. Mater. Interfaces*, 2014, **6**, 7665–7671.

176 M. J. Leeuwner, D. P. Wilkinson and E. L. Gyenge, *Fuel Cells*, 2015, **15**, 790–801.

177 M. Ercelik, M. S. Ismail, D. B. Ingham, K. J. Hughes, L. Ma and M. Pourkashanian, *Energy*, 2023, **262**, 125531.

178 G. Zhang, Z. Qu and Y. Wang, *eTransportation*, 2023, **17**, 100250.

179 Y. Zhang, S. He, X. Jiang, Z. Wang, X. Yang, H. Fang, Q. Li and J. Cao, *Energy*, 2024, **287**, 129664.

180 Y.-H. Lee, S.-M. Li, C.-J. Tseng, C.-Y. Su, S.-C. Lin and J.-W. Jhuang, *Int. J. Hydrogen Energy*, 2017, **42**, 22201–22207.

181 C. Sun, Q. Zuo, G. Hu and Y. Xia, *J. Alloys Compd.*, 2024, 177251.

182 C. Sun, G. Hu, L. Cao, T. Pan, C. Guo and Y. Xia, *ACS Omega*, 2024, **9**, 29797–29804.

183 H. Zhang, K. Peng, J. Dong, L. Zhang, H. Duan, C. Zhao and G. Lin, *J. Appl. Electrochem.*, 2025, **55**, 649–664.

184 H. Song, Y.-T. Liu, X.-f. Zhang, W.-S. Zhang and G.-P. Wu, *Int. J. Hydrogen Energy*, 2024, **92**, 791–800.

185 W. Wang, J. Guo, T. Gu, R. Shi, X. Wei, Q. Zhang, H. Wang and R. Yang, *Energy Fuels*, 2024, **38**, 2368–2376.

186 Z. Wang, K. Wang, K. Jiao, Q. Du, Z. Peng, F. Bai and Z. Liu, *Int. J. Green Energy*, 2025, **22**, 1042–1051.

187 Q. Yin, W. Gao, C. Zhang, F. Gong, Z. Tu, Y. Li, G. Jiang, C. Wang and Z. Mao, *J. Electroanal. Chem.*, 2023, **928**, 117072.

188 F. Cai, S. Cai, S. Li and Z. Tu, *Energy Fuels*, 2024, **38**, 19011–19028.

189 L. Chen, Z. Zhao and R. Lin, *ACS Appl. Mater. Interfaces*, 2025, **17**, 37975–37986.

190 X. Dan, W. li, F. Ning, Q. Wen, L. He, Y. Li, C. He and X. Zhou, *ACS Appl. Energy Mater.*, 2023, **6**, 6019–6028.

191 S. Wang, S. Guan, L. Zhang, F. Zhou, J. Tan and M. Pan, *J. Power Sources*, 2022, **533**, 231402.

192 L. Chen, R. Lin, S. Tang, D. Zhong and Z. Hao, *J. Power Sources*, 2020, **467**, 228355.

193 N. Wu, D. Hou, Q. Zhang, Y. Liu, A. Yao, J. Yang, S. Zhang, R. Song, D. Zhang, Y. Qi, R. Yang and L. Wang, *ACS Sustainable Chem. Eng.*, 2023, **11**, 6545–6555.

194 J. Sun, P. Lin, L. Zeng, Z. Guo, Y. Jiang, C. Xiao, Q. Jian, J. Ren, L. Pan, X. Xu, Z. Li, L. Wei and T. Zhao, *Nat. Commun.*, 2025, **16**, 6528.

195 S. Jang, H.-Y. Park, J. Jung, J. Lee, H.-Y. Park, J. H. Jang, S. M. Kim and S. J. Yoo, *ACS Sustainable Chem. Eng.*, 2019, **7**, 15487–15494.

196 L. Chen, R. Lin, X. Yu, T. Zheng, M. Dong, M. Lou, Y. Ma and Z. Hao, *ACS Appl. Mater. Interfaces*, 2021, **13**, 20201–20212.

197 H. Liu, J. Zhang and B. Wang, *Int. J. Hydrogen Energy*, 2025, **144**, 1–7.

198 H. Liu, Z. Chang, F. Dong, J. Zhang and B. Wang, *J. Power Sources*, 2025, **646**, 237239.

199 Z. Zhu, S. Li, L. Zhang, X. Lu, P. Huang, Y. Wang and M. Pan, *Energy Fuels*, 2023, **37**, 6749–6756.

200 T. Eom, S. Shin, M. Hong, E. S. Lee and S. E. Lee, *J. Mater. Chem. A*, 2025, **13**, 17963–17975.

201 R. Lin, S. Tang, X. Diao, D. Zhong, L. Chen, D. Froning and Z. Hao, *Appl. Energy*, 2020, **274**, 115214.

202 Y. Zhang, S. Lan, M. Lou and R. Lin, *ACS Appl. Mater. Interfaces*, 2025, **17**, 6385–6394.

203 N. Wu, Y. Liu, S. Zhang, D. Hou, R. Yang, Y. Qi and L. Wang, *J. Colloid Interface Sci.*, 2024, **657**, 428–437.

204 X. Cheng, C. He, Q. Wen, Y. Jiang, W. Li, J. Huang, W. Huang, X. Zhu, X. Chu, F. Ning, L. Sun, B. Tian and X. Zhou, *J. Mater. Chem. A*, 2025, DOI: **10.1039/d5ta02041g**.

205 C. Lee, W. J. M. Kort-Kamp, H. Yu, D. A. Cullen, B. M. Patterson, T. A. Arman, S. Komini Babu, R. Mukundan, R. L. Borup and J. S. Spendelow, *Nat. Energy*, 2023, **8**, 685–694.

206 F. Ning, J. Qin, X. Dan, S. Pan, C. Bai, M. Shen, Y. Li, X. Fu, S. Zhou and Y. Shen, *ACS Nano*, 2023, **17**, 9487–9500.

207 J. Huang, B. Peng, T. Stracensky, Z. Liu, A. Zhang, M. Xu, Y. Liu, Z. Zhao, X. Duan and Q. Jia, *Sci. China Mater.*, 2022, **65**, 704–711.

208 S. Mo, L. Du, Z. Huang, J. Chen, Y. Zhou, P. Wu, L. Meng, N. Wang, L. Xing, M. Zhao, Y. Yang, J. Tang, Y. Zou and S. Ye, *Electrochem. Energy Rev.*, 2023, **6**, 28.